Computational Simulations of the 10-MW TP3 Arc-Jet Facility Flow

Tahir Gökçen,* John A. Balboni,† and Antonella I. Alunni‡
NASA Ames Research Center, Moffett Field, CA 94035

This paper reports computational simulations and analysis in support of calibration tests in a high enthalpy arc-jet facility at NASA Ames Research Center. These tests were conducted using stagnation calorimeters and two different blunted wedge models with calibration plates at a wide range of conditions in the NASA Ames 10-MW TP3 facility. Data were obtained using four different conical nozzles with the same test configuration in which the models were placed in a free jet downstream of the nozzle. Experimental surveys of arc-jet test flow with pitot and null-point heat flux probes were also performed at several arc-heater conditions, providing assessment of the flow uniformity and valuable data for the flow characterization. The present analysis comprises computational fluid dynamics simulations of the nonequilibrium flowfield in the facility nozzle and test box, including the models tested, and comparisons with the experimental measurements. These computational simulations provide estimates of the arc-jet test environment parameters that are not measured but are needed to evaluate the performance of thermal protection system materials, along with further valuable insights into the arc-jet testing environment. Simulation results are used to estimate centerline total enthalpy, surface shear, boundary layer thickness, and boundary layer edge Mach number and to verify that specific test requirements from the Orion program are met.

Nomenclature

c_i	=	species mass fraction for species i
D_e	=	nozzle exit diameter, cm (or in)
h	=	enthalpy, MJ/kg
h_o	=	total enthalpy, MJ/kg
h_{ob}	=	mass-averaged total enthalpy (or bulk enthalpy), MJ/kg
h_{ocl}	=	centerline total enthalpy, MJ/kg
h_{oe}	=	boundary-layer edge total enthalpy, $0.995h_{ocl}$ (or $0.995h_{ole}$)
h_{ole}	=	total enthalpy at the wedge leading edge, MJ/kg
I	=	arc current, A
M	=	Mach number
M_e	=	Mach number at boundary layer edge
$\dot{m}$	=	mass flow rate, kg/s
p	=	pressure, kPa
p_{box}	=	test box pressure, torr
p_{midc}	=	arc-heater mid-column pressure, kPa
p_o	=	total pressure, kPa
p_s	=	surface pressure, kPa
p_{t2}	=	pitot pressure, kPa
q_s	=	surface heat flux, W/cm^2
q_{HWFC}	=	hot-wall full-catalytic heat flux, W/cm^2
r_c	=	wedge or model corner radius, m
r_n	=	nose radius, m

* Senior Research Scientist, ERC, Inc., MS 230-2, Associate Fellow AIAA
† Systems Engineer, Arc Jet Consolidation Project, Thermo-Physics Facilities Branch, MS 242-8
‡ Research Scientist, ERC, Inc., MS 234-1, Member AIAA

s = arc-length coordinate or the survey probe location, m
T = temperature or translational-rotational temperature, K
T_v = vibrational-electronic temperature, K
u = axial velocity component, m/s
V = magnitude of velocity vector, m/s
V = arc voltage, V
x_{ml} = model location from the nozzle exit plane, cm
δ = boundary layer thickness based on total enthalpy profile, cm
ρ = density, kg/m^3
τ_s = surface shear, Pa

I. Introduction

The Aerodynamic Heating Facility (AHF) at NASA Ames Research Center (ARC) was recently upgraded to include an additional arc-heater, namely the TP3, which was formerly the TP2 that had been operated at the Johnson Space Center.[1] The TP3 is a 10-MW constricted arc heater and it currently operates with a test gas mixture of pure nitrogen and variable oxygen without argon gas, or with mixtures of nitrogen and carbon dioxide in the future. Recently, a series of arc-jet tests—called Community Acceptance Tests (CAT) were conducted to qualify the 10-MW arc-jet facility for future NASA Orion capsule thermal protection system (TPS) testing.[2] Computational fluid dynamics (CFD) simulations for these tests are performed to provide accurate estimates of the test environment parameters. The centerline total enthalpy of the test flow is estimated using CFD simulations that reproduce measured facility and calorimeter/calibration data. The other test requirements from the Orion program such as boundary layer thickness and boundary layer edge Mach number for wedge tests are also verified through CFD simulations. After the CAT program, surveys of arc-jet test flow with pitot and null-point heat flux probes were performed for flow characterization. The paper describes the computational approach to determine centerline total enthalpy, provides comparisons with the survey data, and gives examples of simulations from the wedge tests to estimate test environment parameters of interest (surface shear, boundary layer thickness and edge Mach number).

II. Arc-Jet Facility and Tests

NASA ARC has four arc-jet facilities within its Arc-Jet Complex. The AHF within this Complex had been operating with two interchangeable arc heaters: a 20-MW constricted arc heater and an optional 20-MW Huels-type arc heater. The AHF was recently upgraded through the arc-jet consolidation project to include a third arc heater, TP3.[2] The TP3 is a 10-MW constricted arc heater originally operated at the Johnson Space Center with the TP2 designation. The TP3, similar to the TP2 operation, is designed to operate with a set of conical nozzles. All of the nozzles have the same inlet diameter of 10.16 cm (4 in), the same throat diameter of 5.715 cm (2.25 in), and varying exit diameters ranging from 12.7 cm to 101.6 cm (5 in to 40 in). The diverging section of each nozzle has a half-angle of 15°.

During CAT, the 10-MW arc heater was operated in the AHF over a wide range of conditions (pressure, mass flow rate, current, mass injection, etc.), using four different conical nozzles with exit diameters of 12.7, 19.05, 50.8, and 101.6 cm (or 5, 7.5, 20, and 40 in). Both stagnation and wedge test configurations were employed. For the stagnation tests, 10.16-cm diameter slug and Gardon gage calorimeters with an iso-q (constant heat flux) shape were used. The iso-q model shape consists of a spherical segment nosecap, with nose radius equal to the model diameter, and a cylindrical body aligned with the flow. The shoulder region of the nosecap is rounded to the cylindrical sides (r_c/r_n = 1/16). For the wedge tests, two different wedge model holders were used. Both wedge model holders are made of copper and water-cooled, and they can accommodate either a calibration plate or a TPS sample plate for testing. The calibration plates were instrumented with five Gardon gage calorimeters and two pressure transducers. The smaller wedge model has a width of 17.98 cm and 1.905 cm nose radius, and it can accommodate 15.24 cm x 15.24 cm (6 in x 6 in) panel test articles, while the larger wedge model has 36.83 cm width and 0.9525 cm nose radius, and is used for 30.48 cm x 30.48 cm (12 in x 12 in) test articles. Details of the facility development and arc-jet tests are described in Ref. 2, and further information on the AHF and other ARC arc-jet facilities can be found in Ref. 3.

Subsequent to CAT, as part of Orion TPS testing, the pitot and null-point heat flux surveys of the TP3 7.5-inch nozzle jet in the test section were done at several arc-heater conditions. These surveys, performed with 15° sphere-

cone stagnation probes (r_n = 9.144 mm or 0.18 in), provide assessment of the flow uniformity and valuable data for arc-jet flow characterization.

III. Computational Approach

Computational analyses of the TP3 arc-jet tests are performed through simulation of nonequilibrium expanding flow in the arc-jet nozzle and supersonic jet, and simulation of the flow in the test box and around the test articles. For all CFD calculations, the Data Parallel Line Relaxation (DPLR) code,[4,5] a NASA Ames in-house flow solver, is used. DPLR has been employed extensively at Ames for hypersonic flight, planetary entry and arc-jet simulations. DPLR provides various options for thermophysical models and formulation. For CFD calculations presented in this paper, two-dimensional axisymmetric or three-dimensional Navier-Stokes equations, supplemented with the equations accounting for nonequilibrium kinetic processes, are used in the formulation. The thermochemical model employed for the arc-jet flow includes five species (N_2 O_2, NO, N, O) and the thermal state of the gas is described by two temperatures (translational-rotational and vibrational-electronic) within the framework of Park's two-temperature model.[6]

The flowfield in an arc-jet facility, from the arc heater to the test section, is a very complex, three-dimensional flow with various nonequilibrium processes occurring. In order to simulate the flowfield, several simplifying assumptions are made, and corresponding numerical boundary conditions are prescribed for CFD simulations. The present computational approach follows our earlier work used for simulation of other arc-jet facilities,[7-10] and it is also briefly described here.

Simulations of the TP3 arc-jet facility flow are started from the nozzle inlet. The total enthalpy and its radial profile at the inlet is prescribed based on the facility and calibration data, and the flow properties at the inlet are assumed to be in thermochemical equilibrium. Measured facility data, namely, the total pressure (arc-heater plenum pressure if available), mass flow rate, and test box pressure, are used as boundary conditions. The calibration data obtained include stagnation calorimeter heat flux and pressure in the freestream for the stagnation tests, and additional water-cooled calibration-plate measurements of cold-wall heat flux and surface pressure at multiple locations for the wedge tests. All metallic surfaces, water-cooled nozzle walls, calorimeter model surfaces (copper slug or Gardon gages), and anodized aluminum calibration plate surfaces are assumed to be fully catalytic to recombination reactions of atomic oxygen and nitrogen at a constant temperature of 500 K. The test box is included in CFD simulations, primarily to account for the free jet expansion formed by the under-expanded flow exiting the nozzle to the test box and its potential effects on model flowfields. The jet expansion within the test box is primarily determined by the test box static pressure, which is one of the facility measurements and is prescribed as a boundary condition.

For specifying the flow properties at the nozzle inlet, an in-house code, Nozzle Throat Conditions, is used.[7] This code was originally developed for specifying flow properties at the nozzle throat, where a supersonic frozen Mach number is assumed. When inflow is supersonic, there is a wide range of conditions and profiles that can be freely specified, and they will be consistent with hyperbolic governing equations. However, when the inflow is subsonic, one characteristic relationship is required to specify the inlet flow properties. Since the characteristic relations are not used in the formulation, all of the inlet flow properties can be specified only when they are physically consistent. In other words, not all of the boundary conditions used for supersonic inflow can be used for subsonic inflow. For the nonuniform inlet profile simulations in this paper, pressure at the nozzle inlet is prescribed and assumed to be uniform, and for a given assumed inlet enthalpy profile, the flow properties are calculated from thermochemical equilibrium relations. There is no single enthalpy profile that can be prescribed at the inlet for all conditions even for a given facility because the extent of flow nonuniformity at the inlet is not known and it depends on various factors: facility (or arc-heater design), arc current, arc-heater pressure (or mass flow rate), and cold-gas injection in the plenum, etc. The measured facility data including mass flow rate, bulk enthalpy, and arc-heater pressure are used as constraints on any flow profiles prescribed. The flow nonuniformity at the nozzle exit can be assessed through detailed pitot pressure and heat flux surveys of the flow exiting the nozzle, resulting in an inferred total enthalpy profile that can be used at the nozzle inlet. For most cases, such surveys are not available. At the inlet, although the inlet enthalpy profile is not known, a parabolic enthalpy profile and uniform pressure are assumed such that bulk and centerline values are consistent with the facility total bulk enthalpy estimates, mass flow rate measurements, and

calorimeter heat flux and pressure data. The centerline total enthalpy value is obtained iteratively to reproduce the calorimeter data. The use of a parabolic enthalpy profile at the nozzle inlet requires experimental justification. For that purpose, comparisons of CFD predictions with the available survey data will be presented in the next section.

IV. Computational Simulations

A. Stagnation model simulations and flow surveys

The majority of arc-jet simulations performed are stagnation model simulations. Stagnation calorimeters are often used to calibrate the test conditions and to infer the centerline total enthalpy of the arc-jet flow. First, the stagnation simulations in support of CAT program will be summarized. Then, comparisons of computations with the pitot and null-point heat flux surveys obtained in the TP3 7.5-inch nozzle will be presented.

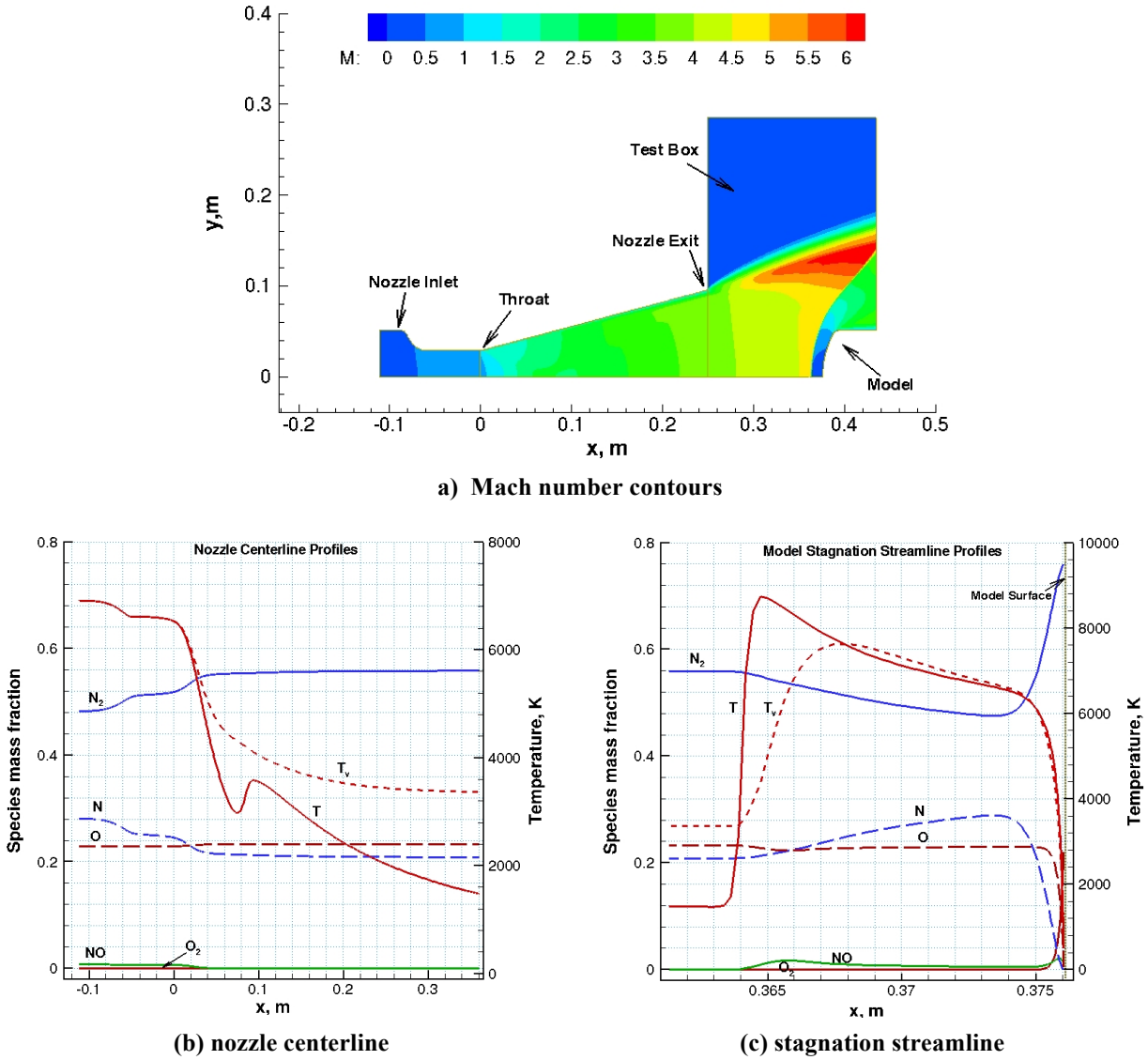

a) Mach number contours

(b) nozzle centerline **(c) stagnation streamline**

Figure 1. Computed TP3 7.5-inch nozzle flowfield including the test box and a 4-inch diameter iso-q calorimeter model: $\dot{m}$ = 201 g/s, h_{ob} = 14.6 MJ/kg, h_{ocl} = 22.3 MJ/kg.

i. Stagnation model simulations

As an illustration of a typical axisymmetric simulation, Fig. 1 shows a computed TP3 7.5-inch nozzle flowfield including the test box and a stagnation calorimeter model. Because of the nonequilibrium expansion process in arc-jet nozzles, the chemical composition freezes near the throat where the flow is dissociated and vibrationally excited. As shown in Fig. 1b, the computations predict that, as expected, the flow is chemically and vibrationally frozen before it reaches the nozzle exit. Note that oxygen remains fully dissociated within the entire flowfield except in the boundary layer near the walls, while nitrogen is partially dissociated. It should be pointed out that the translational temperature rise just downstream of the throat in Fig. 1b is due to a weak oblique shock formation resulting from this particular nozzle throat design, and it is present in all simulations.

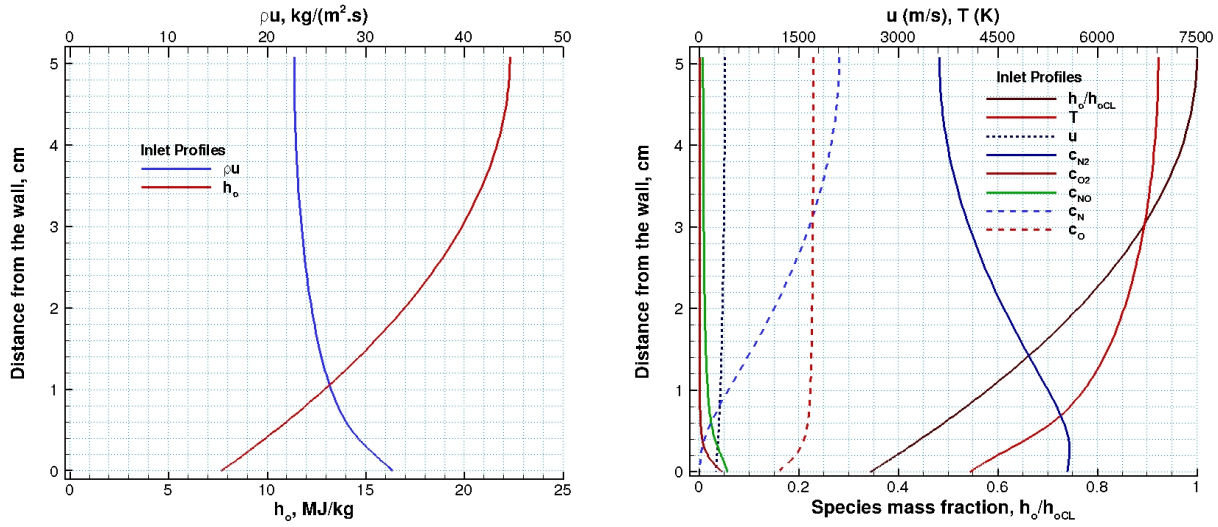

(a) **(b)**

Figure 2. Prescribed inlet profiles to reproduce the 4-inch iso-q calorimeter data. TP3 7.5-inch nozzle flow: $\dot{m}$ = 201 g/s, h_{ob} = 14.6 MJ/kg, h_{ocl} = 22.3 MJ/kg.

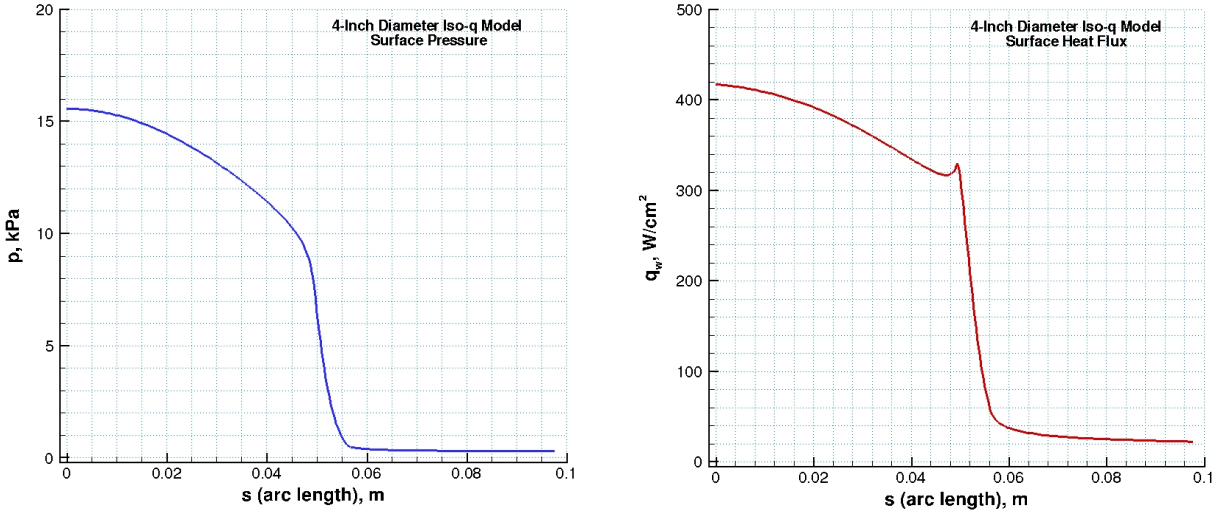

(a) pressure **(b) heat flux**

Figure 3. Computed surface pressure and heat flux distributions for the iso-q model. TP3 7.5-inch nozzle flow: $\dot{m}$ = 201 g/s, h_{ob} = 14.6 MJ/kg, h_{ocl} = 22.3 MJ/kg. Test data (IST Run 39-1): 417 W/cm^2 and 15.6 kPa.

The primary objective of the stagnation model calculations is to estimate the centerline total enthalpy of the arc-jet flow consistent with the facility and calibration measurements. Uniform pressure and a nonuniform parabolic enthalpy profile are specified at the nozzle inlet such that the centerline calibration data are reproduced with the computations. Figure 2 shows inlet profiles of total enthalpy and mass flux and resulting equilibrium species mass fractions and other flow properties prescribed for this case.

Figure 3 shows corresponding computed model surface quantities for this case. It is important to reproduce both experimental surface pressure and heat flux in order to estimate the centerline total enthalpy from CFD simulations.

A large number of stagnation cases from the CAT series are computed to estimate the centerline total enthalpy of the TP3 arc-jet flow. Table 1 summarizes facility conditions and CFD estimated parameters, specific to verification of CAT stagnation test requirements.

Table 1. Summary of facility conditions and CFD estimated parameters for stagnation tests: TP3 5-inch, 7.5-inch, and 20-inch nozzles using 4-inch diameter iso-q calorimeters.

5-inch nozzle

Test Series: IST, AHF 304	x_{ml} **(cm)**	I **(A)**	V **(V)**	$\dot{m}$ **(g/s)**	p_{midc} **(kPa)**	q_s **(W/cm^2)**	p_s **(kPa)**	h_{ocl} **(MJ/kg) CFD**	q_{HWFC} **(W/cm^2) CFD**
AHF 304 Run 60-2	20.32	302	769	160	61	16	5.4	2.28	9.2
IST Run 44-2	12.7	614	2007	349	167	37	13.3	3.0	21
IST Run 14-4	12.7	515	2809	201	140	132	18.3	7.5	95
IST Run 18-1	12.7	518	2776	278	158	93	21.1	5.3	60
AHF 304 Run 48-1	12.7	419	2195	525	207	56	30.9	3.0	28
IST Run 27-1	12.7	614	3048	736	327	99	42.7	4.2	55
IST Run 28-2	12.7	654	3800	679	354	135	46.4	5.2	80

7.5-inch nozzle

Test Series: IST	x_{ml} **(cm)**	I **(A)**	V **(V)**	$\dot{m}$ **(g/s)**	p_{midc} **(kPa)**	q_s **(W/cm^2)**	p_s **(kPa)**	h_{ocl} **(MJ/kg) CFD**	q_{HWFC} **(W/cm^2) CFD**
Run 39-1	12.7	1017	3234	201	209	417	15.6	22.3	356
Run 39-2	12.7	224	1000	18	17	66	1.7	11.7	56
Run 40-1	12.7	861	2886	197	169	163	12.4	10.8	127

20-inch nozzle

Test Series: AHF 304	x_{ml} **(cm)**	I **(A)**	V **(V)**	$\dot{m}$ **(g/s)**	p_{midc} **(kPa)**	q_s **(W/cm^2)**	p_s **(kPa)**	h_{ocl} **(MJ/kg) CFD**	q_{HWFC} **(W/cm^2) CFD**
Run 36-1-3	15.24	423	1220	62	40	14	0.6	5.1	11.3

Table 2. Summary of calibrated facility conditions and CFD estimated parameters: four flight heating profile simulations using the TP3 5-inch nozzle using 4-inch iso-q calorimeters.

Heating Profile 1

Test Series: IST	I (A)	V (V)	$\dot{m}$ (g/s)	p_{midc} (kPa)	q_s (W/cm^2)	p_s (kPa)	h_{ocl} (MJ/kg) CFD	q_{HWFC} (W/cm^2) CFD	Profile Steps
Run 22-1	525	1173	63	42	65	5.7	6.7	48	step 1
Run 23-2	589	2558	137	113	259	14.7	14.5	209	step 2
Run 35-5	1017	4811	517	431	503	49.3	15.4	397	step 3
Run 35-1	1012	4597	562	434	306	56.1	9.5	218	step 4
Run 22-3	526	2996	374	201	87	26.5	4.6	53	step 5

Heating Profile 2 (High Enthalpy)

Test Series: AHF 304	I (A)	V (V)	$\dot{m}$ (g/s)	p_{midc} (kPa)	q_s (W/cm^2)	p_s (kPa)	h_{ocl} (MJ/kg) CFD	q_{HWFC} (W/cm^2) CFD	Profile Steps
Run 43-1	366	1002	22	22	111	3.6	12.9	92	step 1
Run 43-2	725	1656	50	55	317	8.0	22.7	274	step 2
Run 43-3	1006	1764	60	69	441	9.8	27.7	385	step 3
Run 43-4	520	3263	179	155	318	20.5	15.1	256	step 4
Run 43-5	320	1467	31	32	136	5.0	13.2	112	step 5

Heating Profile 3

Test Series: IST	I (A)	V (V)	$\dot{m}$ (g/s)	p_{midc} (kPa)	q_s (W/cm^2)	p_s (kPa)	h_{ocl} (MJ/kg) CFD	q_{HWFC} (W/cm^2) CFD	Profile Steps
Run 22-1	525	1173	63	42	65	5.7	6.7	48	steps 1
Run 25-1	808	2343	131	113	273	15.0	15.1	222	steps 2 & 4
Run 29-1	1015	3348	239	231	576	29.6	21.7	487	step 3
Run 24-2	410	2519	141	99	135	13.0	8.8	102	step 5
Run 20-3	302	1459	45	39	64	5.4	5.1	32	step 6
Run 26-3	681	2877	247	165	117	21.0	6.4	79	step 7

Heating Profile 4 (High Enthalpy)

Test Series: AHF 304	I (A)	V (V)	$\dot{m}$ (g/s)	p_{midc} (kPa)	q_s (W/cm^2)	p_s (kPa)	h_{ocl} (MJ/kg) CFD	q_{HWFC} (W/cm^2) CFD	Profile Steps
Run 38-1	509	1149	32	42	70	6.3	6.8	52	steps 1 & 6
Run 45-3	1006	1336	40	48	341	6.8	26.0	298	step 2
Run 45-4	1211	2045	80	94	576	13.2	30.8	506	step 3
Run 45-5	615	1800	50	55	307	8.1	21.9	264	step 4
Run 45-7	412	1139	23	25	169	4.0	17.8	145	step 5
Run 40-8	725	3127	267	189	158	25.5	7.6	111	step 7

For all 5-inch nozzle heating profile conditions, the calorimeter location is at x_{ml} = 12.7 cm.

Table 3. Summary of calibrated facility conditions and CFD estimated parameters: one flight heating profile simulation using the TP3 7.5-inch nozzle and 4-inch iso-q calorimeters.

Heating Profile 5

Test Series: AHF 305	I (A)	V (V)	$\dot{m}$ (g/s)	p_{midc} (kPa)	q_s (W/cm^2)	p_s (kPa)	h_{ocl} (MJ/kg) CFD	q_{HWFC} (W/cm^2) CFD	Profile Steps
Run 1-1	352	942	22	23	61	1.2	12.9	52	step 1
Run 2-2	916	1572	50	57	193	2.9	23.9	170	step 2
Run 1-3	1607	3884	300	338	466	16.6	24.3	401	step 3
Run 1-4	811	3796	270	250	272	12.1	17.5	228	step 4
Run 2-5	521	3106	220	157	74	8.0	6.8	54	step 5

Calorimeter location is at x_{ml} = 22.86 cm.

One of the objectives of the CAT series was to demonstrate an arc-jet testing capability to simulate various heating profiles in time representative of Orion flight. Summaries of the calibrated facility conditions for several heating profiles including the estimated hot-wall heat flux and centerline total enthalpy values are given in Tables 2 and 3. Each particular profile was broken into independent steps, from 5 to 7 steps where each step was calibrated for its centerline conditions prior to a flight profile run, and subsequently the heating profile simulation was demonstrated in a single arc-jet run. Several trade-offs are usually made in order to simulate a flight heating profile in an arc-jet test, a subject which is outside the scope of this paper. However, in general, for a flight heating profile simulation, the hot-wall fully-catalytic heat flux profile and total heat load predicted for a flight trajectory are duplicated in an arc-jet test. Various compromises are made in terms of surface pressure and total enthalpy profiles within the operating envelop of the facility. For instance, the heat flux levels of many steps used in heating profile 2 are similar to those used in heating profile 1 but they are achieved at higher enthalpies and lower surface pressures. Likewise, heat flux levels of heating profiles 3 and 4 are somewhat similar but at different enthalpies and surface pressures.

In our earlier work,[7,9] it was shown that the deduced centerline total enthalpy value is not sensitive to the enthalpy profile prescribed at the nozzle inlet (or throat), as long as model surface pressure and heat flux measurements are reproduced by the computations. However, a nonuniform enthalpy profile is usually needed to be consistent with the mass-averaged (or bulk) facility parameters, namely, mass flow rate and bulk enthalpy. Nevertheless, in order to use any specific enthalpy profile at the nozzle inlet, some experimental justification is needed. Although there is no single enthalpy profile that can be used for all arc-jet conditions, a parabolic enthalpy profile, with different centerline-to-bulk enthalpy ratios depending on the facility data, is found to be adequate to reproduce available survey data obtained at the model location downstream of the nozzle exit. Examples of nozzle exit surveys, and comparisons of computations with the data are given below.

ii. Comparisons with survey data

The pitot and null-point heat flux surveys of the TP3 7.5-inch nozzle jet were performed using 15° sphere-cone probes (r_n = 9.144 mm or 0.18 in). The sweeps to survey across the nozzle were done by moving the probes horizontally across the free jet in two directions: first from west to east, then retracting back east to west. This provide two experimental data sets for each survey sweep. Further information on the survey probes can be found in Ref. 11. Direct comparisons of CFD simulations with the survey data have various challenges. Three dimensional CFD simulations of flowfields around the survey probes would be required at several locations in the test section. Furthermore, while for the pitot pressure surveys the obtained data are quantitative, for the null-point heat surveys the heat flux measurements were provided as qualitative measurements, and only normalized distributions of heat flux can be used in comparisons. For the present paper, approximate comparisons are made based on the computed CFD flowfields. Quantitative pitot pressure comparisons are based on the computed flowfield and shock relations (pressure, Mach number, frozen flow). For comparisons of the normalized heating distributions, the heat flux to the null-point probe is assumed to be proportional to $h_o\, p_{t2}^{1/2}$, and computed based on the CFD flowfield.

Comparisons of computations with the pitot and null-point heat flux survey data will be presented for four cases. Note that for each case, the centerline total enthalpy value is set such that centerline stagnation calorimeter data,

surface pressure and heat flux are reproduced. The survey data were obtained in separate arc-jet runs but at the same nominal facility conditions listed in Table 4, and are plotted in Figs. 4-7. Also, note that the pitot survey data were taken during a different run from the null-point heat flux surveys, at nominally the same arc heater settings (mass flow rate and arc currents).

Table 4. Summary of nominal facility conditions for four cases: stagnation calorimeter data and CFD estimated parameters for the nozzle exit surveys in the TP3 7.5-inch nozzle using 4-inch diameter flat-faced calorimeters (r_c/r_b = 3/16) with data obtained at x_{ml} = 15.24 cm.

Test Series: AHF 307	I (A)	V (V)	$\dot{m}$ (g/s)	p_{midc} (kPa)	q_s (W/cm^2)	p_s (kPa)	h_{ocl} (MJ/kg) CFD	q_{HWFC} (W/cm^2) CFD	Pitot and Null-Point Surveys
Runs 3-2, 4-1	419	1683	40	43	118	3.3	19.6	104	case 1
Runs 11-2, 12-2	1113	3401	190	220	388	14.7	28.8	349	case 2
Runs 6-1, 7-1	1214	3946	310	311	335	21.5	21.9	292	case 3
Runs 3-3, 4-2	716	3681	310	251	114	17.0	9.4	89	case 4

The first case, shown in Fig. 4, represents a facility condition at a relatively low mass flow rate and moderate enthalpy. There is no plenum cold gas injection. It should be noted that both pitot and heat flux survey data are not symmetric with respect to the nozzle centerline, while the obtained sweep data are repeatable in both sweep directions. It is not clear what the source of this asymmetry in the flow is, and obviously any observed asymmetry in the flow cannot be reproduced by an axisymmetric formulation. Also note that there was not a complete recovery in the pitot data to the test box pressure (most likely because the pitot survey probe was moving too fast to equililbrate at these low pressures). Nevertheless, the present axisymmetric simulations with the specified parabolic profile reproduce the survey data reasonably well.

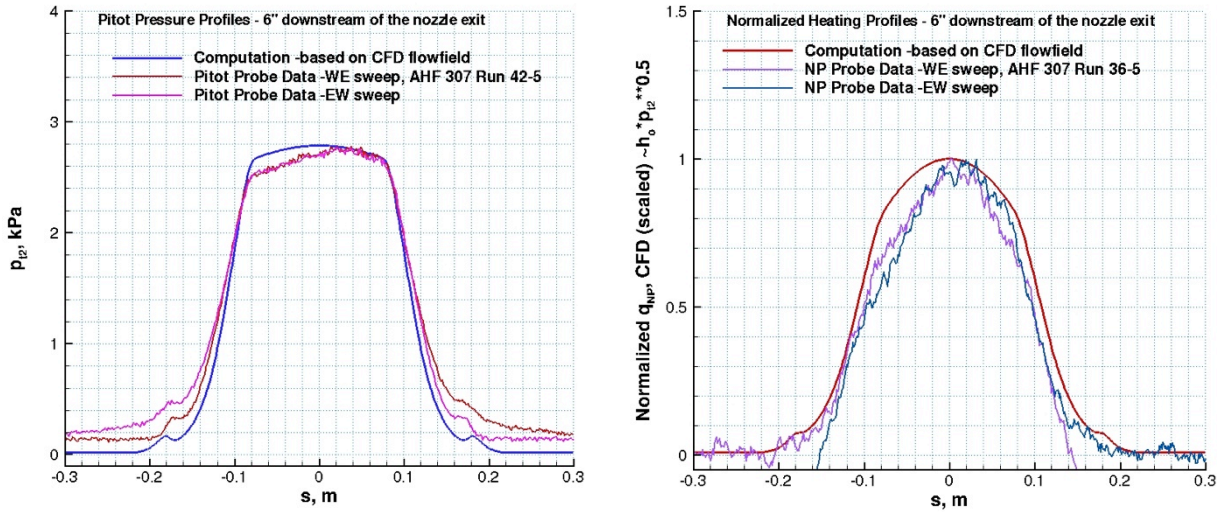

(a) pitot pressure **(b) normalized heat flux**

Figure 4. Comparisons of computations with the pitot and null-point heat flux survey data (case 1). TP3 7.5-inch nozzle flow: $\dot{m}$ = 40 g/s, h_{ob} = 15.4 MJ/kg, h_{ocl} = 19.6 MJ/kg, p_{box} = 0.1 torr.

The second case, shown in Fig. 5, represents a facility condition at an intermediate mass flow rate, relatively high enthalpy and without plenum gas injection. Note that the extent of asymmetry in both pitot and heat flux data is smaller than in the first case (within the measurement fluctuations). Note also that there appears to be some variation in the pitot pressure, possibly resulting from weak wave interactions in the supersonic jet. Again, the present axisymmetric simulations reproduce the survey data quite well.

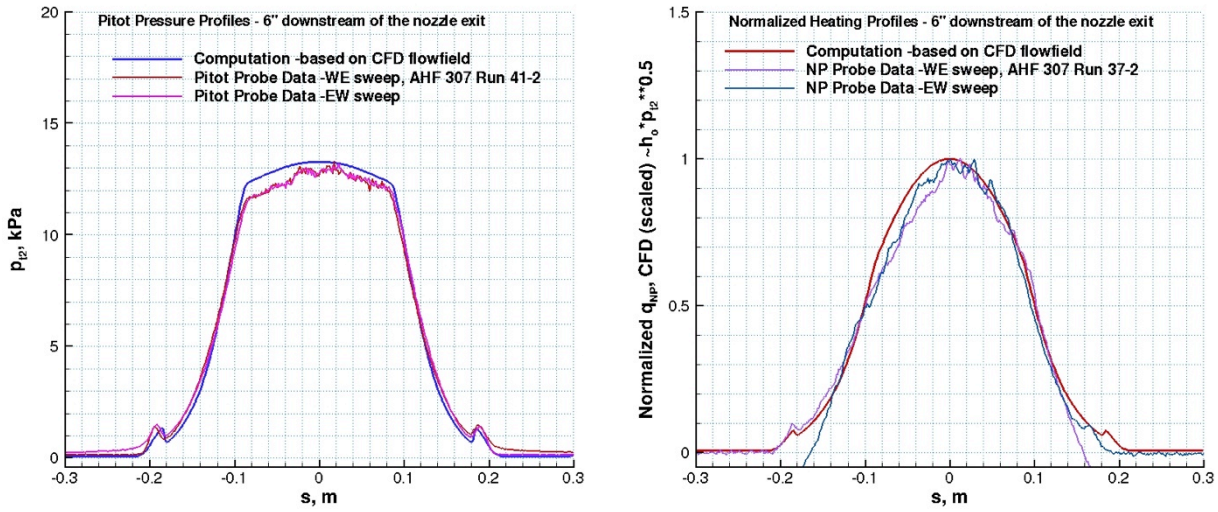

(a) pitot pressure **(b) normalized heat flux**

Figure 5. Comparisons of computations with the pitot and null-point heat flux survey data (case 2). TP3 7.5-inch nozzle flow: $\dot{m}$ = 190 g/s, h_{ob} = 17.6 MJ/kg, h_{ocl} = 28.8 MJ/kg, p_{box} = 0.4 torr.

The third case, shown in Fig. 6, represents a facility condition at a relatively high mass flow rate and moderately high enthalpy with plenum gas injection of N_2. For this case, the pitot pressure survey shows a somewhat higher pressure region near the nozzle centerline but both surveys appear to be approximately symmetric. Again, both pitot and heat flux survey data are reasonably well reproduced by the CFD simulations.

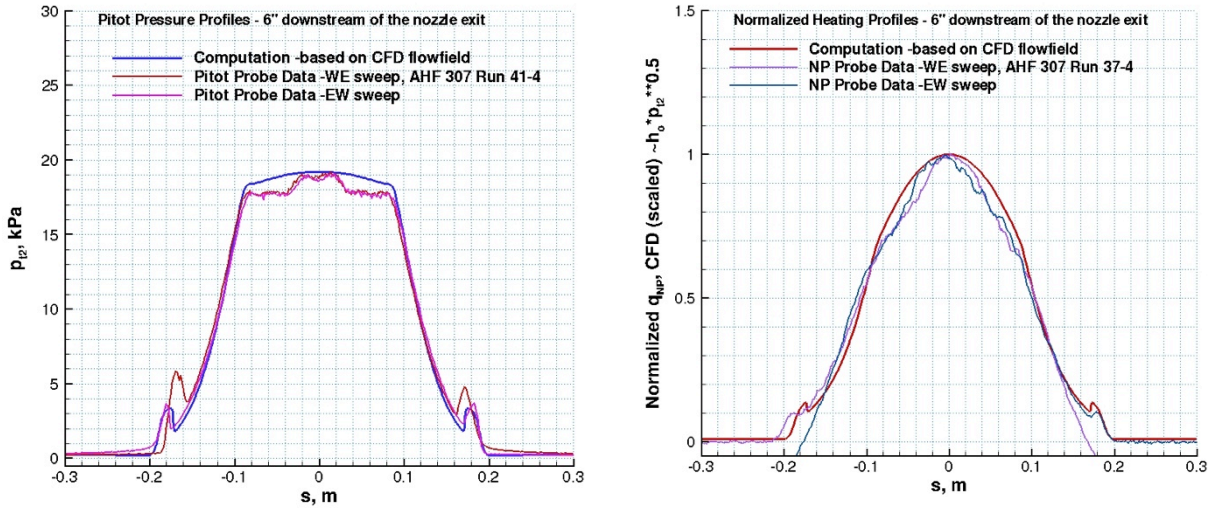

(a) pitot pressure **(b) normalized heat flux**

Figure 6. Comparisons of computations with the pitot and null-point heat flux survey data (case 3). TP3 7.5-inch nozzle flow: $\dot{m}$ = 310 g/s, h_{ob} = 13.6 MJ/kg, h_{ocl} = 21.9 MJ/kg, p_{box} = 1 torr.

The fourth case, shown in Fig. 7, represents a facility condition at a relatively high mass flow rate and relatively low enthalpy. The mass flow rate for this case is the same as the third case but the centerline total enthalpy is much lower. The lower enthalpy is achieved through a lower arc current and more cold gas injection of N_2 at the plenum. It should be noted that the features in the pitot and heat flux surveys (at s ~ ±0.15 for pressure, and s ~ ±0.19 for heat flux) correspond to the nozzle jet boundary which location is primarily determined by the test box pressure. The pressure and heat flux surveys were obtained in two separate runs at the same nominal arc-heater conditions. However, the box pressures for each run were different. While the pitot pressure survey appears to indicate some wave interactions near the nozzle centerline, the computations are in good agreement with the survey data.

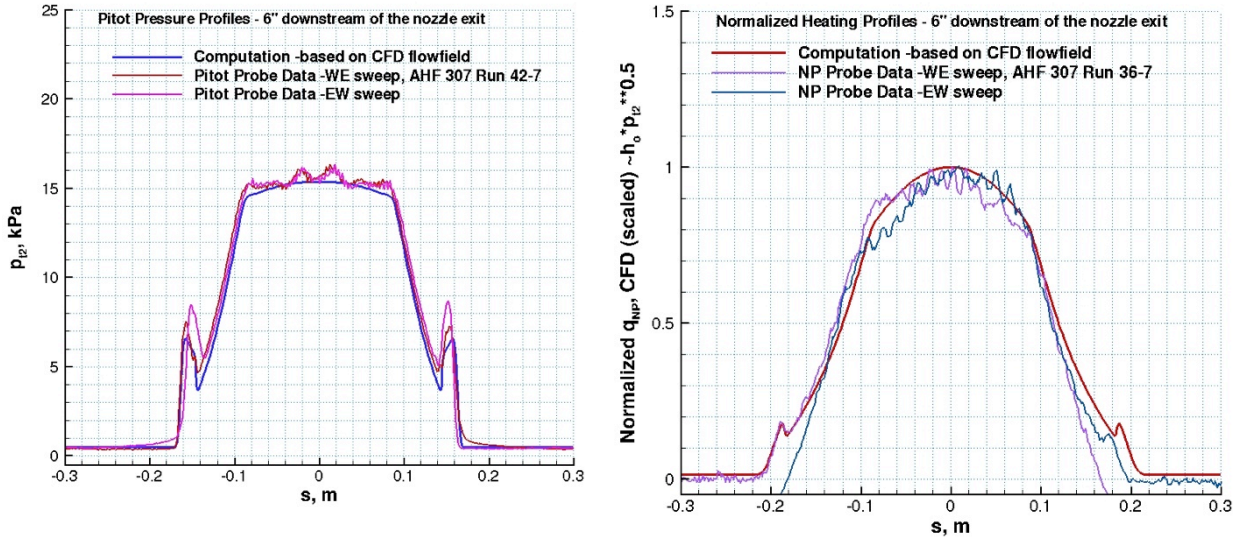

(a) pitot pressure at p_{box} = 2 torr **(b) normalized heat flux at p_{box} = 0.5 torr**

Figure 7. Comparisons of computations with the pitot and null-point heat flux survey data (case 4). TP3 7.5-inch nozzle flow: $\dot{m}$ = 310 g/s, h_{ob} = 7.5 MJ/kg, h_{ocl} = 9.4 MJ/kg, p_{box} = 0.5-2 torr.

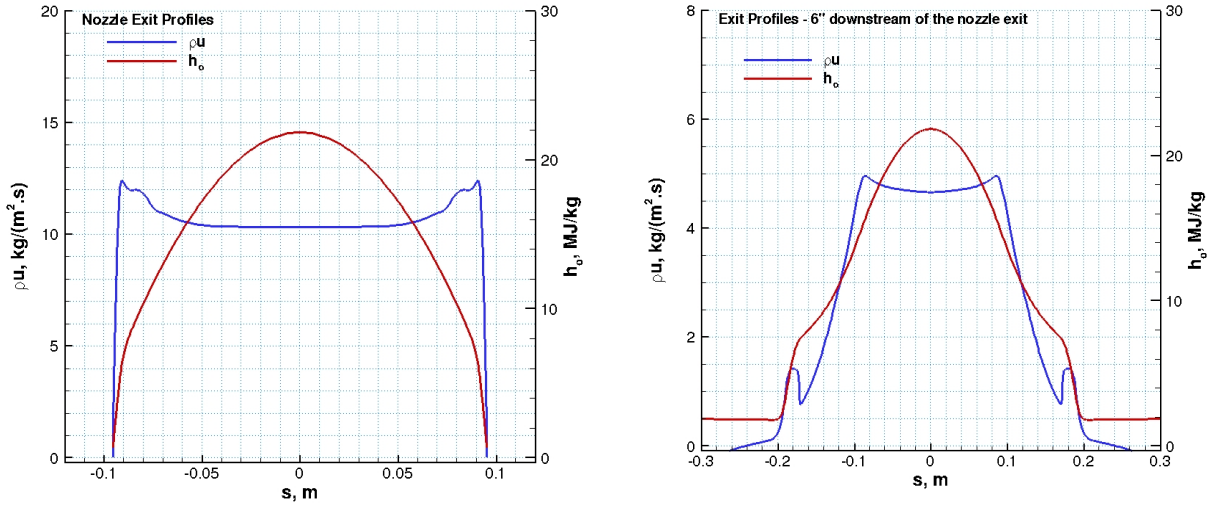

(a) **(b)**

Figure 8. Computed mass flux and total enthalpy profiles at the nozzle exit and survey location (case 3). TP3 7.5-inch nozzle flow: $\dot{m}$ = 310 g/s, h_{ob} = 13.6 MJ/kg, h_{ocl} = 21.9 MJ/kg, p_{box} = 1 torr.

It should be pointed out here that the heating profile measured by the survey probes does not represent the total enthalpy profile. (The heating profile corresponds approximately to the total enthalpy profile only if the pitot pressure profile is uniform.) In the literature, e.g., notably Pope[12] and others, it is often postulated that one can deduce the enthalpy profile from the pitot and heat flux surveys with simplfying assumptions. Any such methodology requires knowledge of the mass flux profile at the location at which such surveys are made. Pope assumed that the mass flux profile was uniform to simplify the analysis. For some cases, a similar methodology is used assuming a specific mass flux profile (e.g., proportional to the pitot pressure or an empirical relation). Since there is no one mass flux profile that can be assumed for all cases, the most reliable approach is through direct comparisons of computed flowfield properties with the measurements. As an example, in Fig. 8, computed mass flux and enthalpy profiles are shown for two axial locations in the same free jet as for case 3. Figure 8b corresponds to the same axial distance as the data in Fig. 6. It is clear that the mass flux profile in Fig. 8b is neither uniform nor

similar to the pitot pressure profile shown in Fig. 6. It should also be noted that determination of any integrated quantity such as mass-averaged bulk enthalpy requires distributions of mass flux and total enthalpy not only in the inviscid core but also in the shear layer in the test box at the survey location.

B. Wedge model simulations

Testing of TPS panel samples by making use of a blunted wedge holder with a conical nozzle is one of the frequently employed arc-jet test configurations. In order to characterize the heating environment over the panel test article, a calibration plate with the same geometry as the test article is usually instrumented with an array of heat flux calorimeters and pressure gages. The primary objective of CFD simulations for the wedge tests is to provide estimates of various surface and flow quantities of interest such as surface shear, boundary layer thickness and boundary layer edge Mach number (M_e). For some cases, boundary layer thickness and M_e , along with surface presssue and heat flux range, were specified as the test requirements, and these can be verified only through CFD simulations, as no experimental techniques are known to measure them in these high enthalpy conditions.

As mentioned earlier, two different wedge model holders were used in two different nozzles. The smaller wedge model was used in the 7.5-inch nozzle for testing 15.24 cm x 15.24 cm (6 in x 6 in) panel test articles, while the larger wedge model was used in the 20-inch nozzle for testing 30.48 cm x 30.48 cm (12 in x 12 in) test articles. Examples from both wedge configurations are given.

i. TP3 7.5-inch nozzle flow/wedge model simulations

Two examples from simulations of the smaller wedge in the 7.5-inch nozzle are given. The two wedge cases differ in terms of heating levels, the extent of flow nonuniformity in the test flow (different bulk to centerline enthalpy ratios), and the location of the wedge test article with respect to the nozzle centerline. Nominal surface heat flux and pressure requirements for the water-cooled calibration plate were 50 W/cm^2 and 9.6 kPa for the first case, and 272 W/cm^2 and 15 kPa for the second case. The results for the first case are given in Figs. 9-13, and for the second case in Figs. 14-17. The wedge half-angle was 45° in both cases.

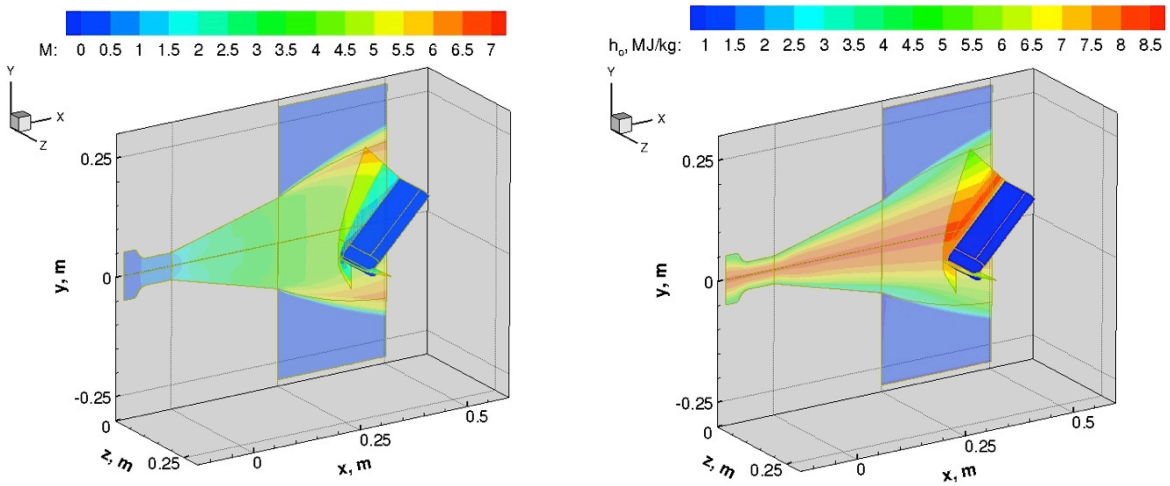

(a) Mach number **(b) total enthalpy**

Figure 9. Computed flowfield contours of the TP3 7.5-inch nozzle flow and test box with the 45° wedge model: $\dot{m}$ = 296 g/s, h_{ob} = 6.0 MJ/kg, h_{ocl} = 8.1 MJ/kg , p_{box} = 2 torr.

Figure 9 shows the computed Mach number and total enthalpy contours of the TP3 7.5-inch nozzle flow downstream of the nozzle inlet for the first case. The contours are shown on the x-y symmetry planes of the nozzle flowfield and on other planes of interest for the flowfield of the test box and over the wedge model. The expansion waves emanating from the nozzle lip at the exit to the test box ordinarily affect the shape and strength of the shock formed over the wedge model, thus affecting the pressure distribution on the model. For this case, the wedge model was therefore tested at an off-centerline location (the leading edge of the wedge model is at 15.24 cm downstream of

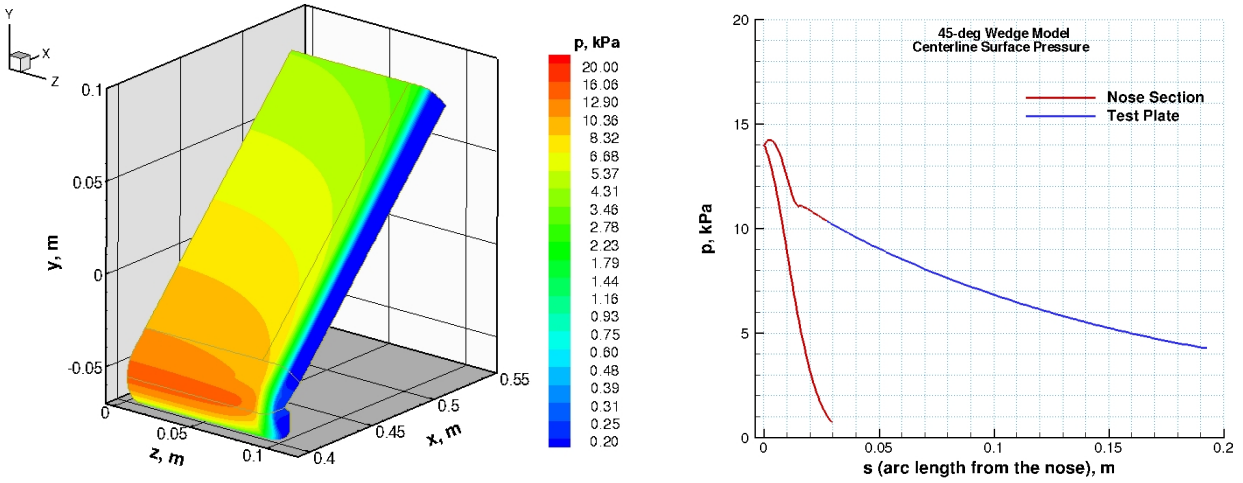

(a) pressure

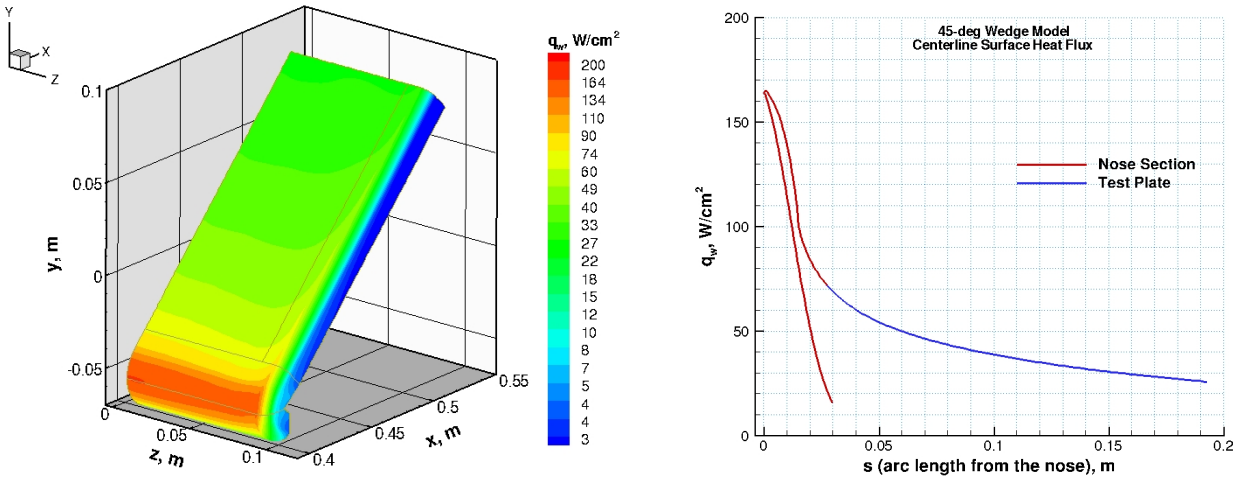

(b) heat flux

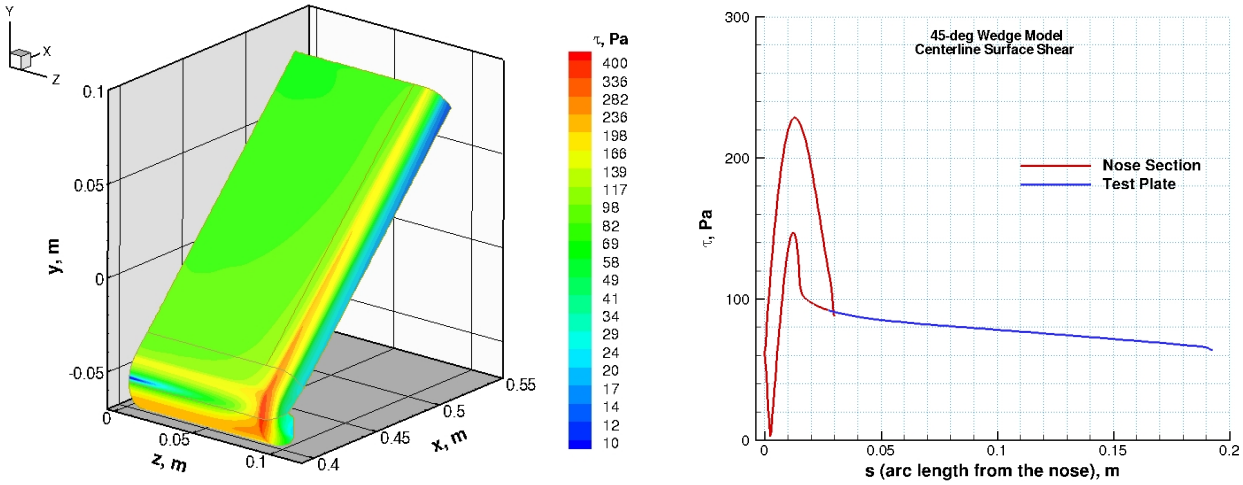

(c) shear

Figure 10. Computed surface quantities of the 45° wedge model. TP3 7.5-inch nozzle flow: $\dot{m}$ = 296 g/s, h_{ob} = 6.0 MJ/kg, h_{ocl} = 8.1 MJ/kg.

the nozzle exit and 5.72 cm below centerline) in order to reduce the effects of the expansion wave on the model surface pressure.

Figure 10 shows contours of the computed surface quantities (pressure, heat flux, and shear) of the wedge model and their centerline profiles for the first condition described. Note that the surface pressure drops significantly along the wedge centerline. (In contrast, a two-dimensional blunted wedge simulation–not shown–with uniform freestream results in approximately constant pressure distribution on the wedge surface.) The pressure drop observed along the test plate centerline is due to the following two factors: three-dimensional conical flow expansion over the side of the model (cross flow effects), and interaction of the expansion waves from the nozzle exit with the bow shock wave of the wedge model. As expected, the effect of the expansion wave becomes increasingly dominant when the model size and the nozzle exit diameter are comparable. It should be noted here that the stagnation point of the wedge flowfield is no longer at the wedge leading edge location. This is clearly seen from the computed surface plots in Fig. 10; particularly note that the peak surface pressure in Fig. 10a, and the minimum surface shear in Fig 10c are not at the leading edge. This is due to the fact that the leading edge of the wedge model is not at the nozzle centerline. Because of the conical expansion in the nozzle, the flow approaching the leading edge has not only an axial velocity component but also includes a radial component.

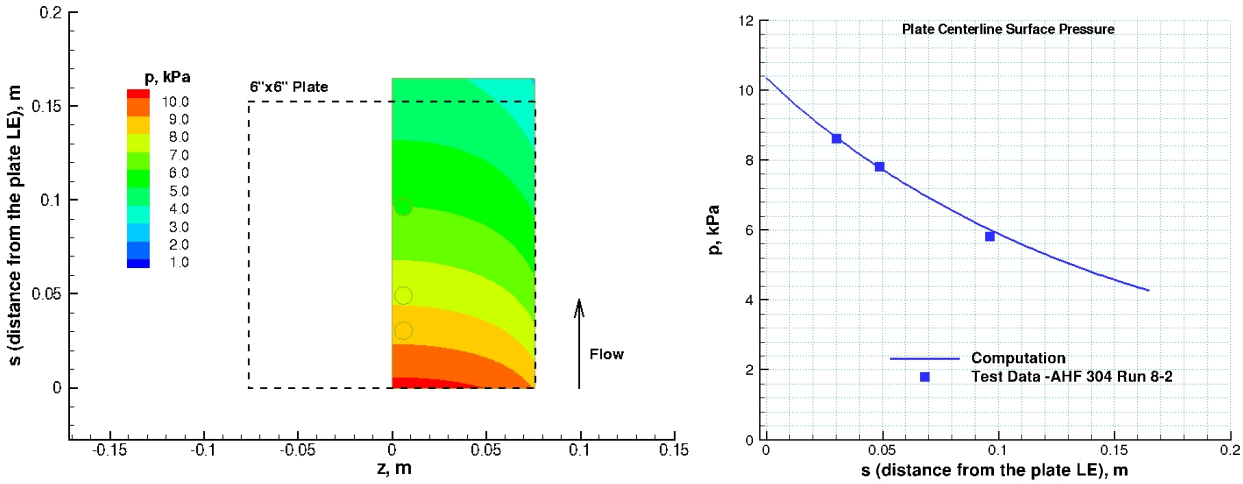

(a) pressure

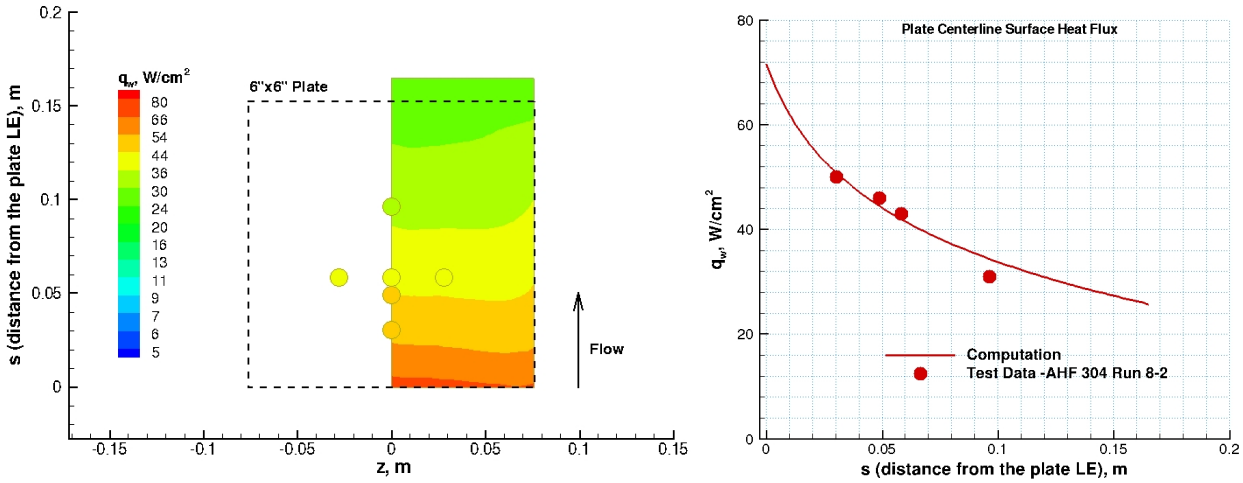

(b) heat flux

Figure 11. Comparisons of computed surface pressure and heat flux of the calibration plate with the test data for the 45° wedge model. TP3 7.5-inch nozzle flow: $\dot{m}$ = 296 g/s, h_{ob} = 6.0 MJ/kg, h_{ocl} = 8.1 MJ/kg.

Figure 11 shows comparisons of computed calibration-plate surface quantities with the test data. The contour plots show computed surface pressure and heat flux on one half of the calibration plate, and the symbols in the contour plots are the measurements, color coded with the same contour levels. The line plots show the corresponding profiles along the plate centerline, including the measurements. A complete uncertainty analysis of the calibration plate measurements is not available. However, based on empirical evidence (historical Ames arc-jet data with similar measurements), the heat flux measurements are estimated to be accurate to within ±15% and the pressure measurements to within ±5%. Note that both computed and measured surface pressure and heat flux values are in agreement. The agreement in the rate of pressure drop along the plate centerline indicates that wave interaction and three dimensional effects are adequately captured by the computations.

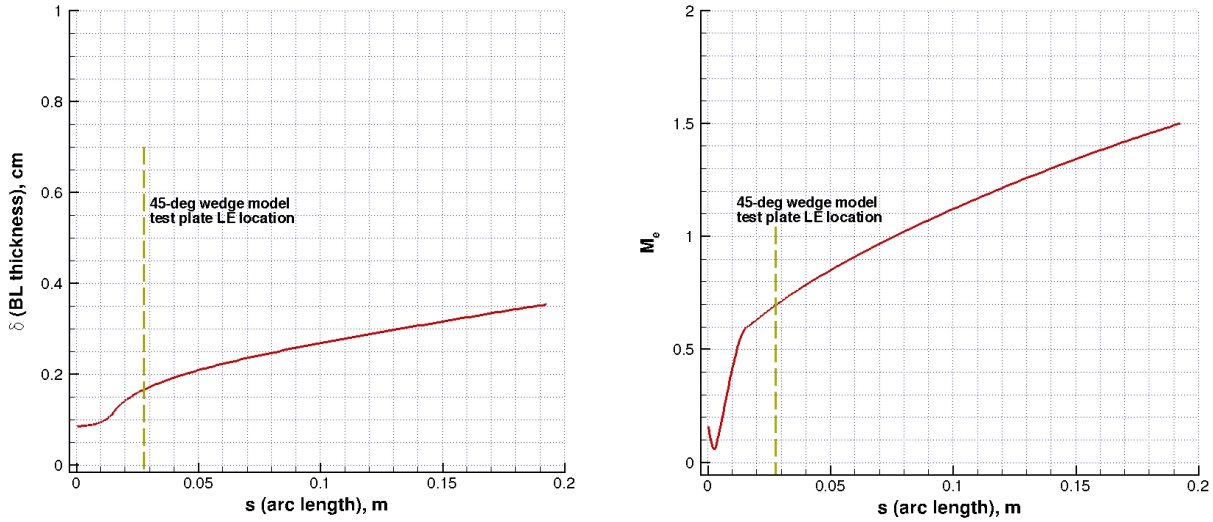

Figure 12. Computed boundary layer thickness and edge Mach number along the 45° wedge model centerline. TP3 7.5-inch nozzle flow: $\dot{m}$ = 296 g/s, h_{ob} = 6.0 MJ/kg, h_{ocl} = 8.1 MJ/kg.

Figure 12 shows the distributions of the predicted boundary layer thickness and edge Mach number along the model centerline. The boundary layer thickness and edge Mach number are often important to evaluate the performance of TPS materials. The Orion program had specific test requirements on these quantities for the wedge tests. For instance, one of the test requirements was to achieve a subsonic boundary layer edge Mach number at the plate leading edge. These requirements are verified only through these CFD simulations.

Determination of the boundary layer edge thickness for the wedge flowfields deserves some clarification. For a high enthalpy reacting flow, several boundary layer thicknesses can be defined in terms of momentum, temperature, enthalpy, and species concentrations, etc. However, as there are flowfield gradients in all of these quantities, the total enthalpy profile normal to the wall is usually used to detect the boundary layer edge. One method often used is that as one marches away from the wall, the location at which $h_{oe} = 0.995\, h_o$ is determined as the boundary layer edge (e.g., see BLAYER program[12]). Clearly, this definition is an approximation (not meant to be precise) and an attempt to provide a consistent boundary layer thickness estimate of a high enthalpy flow for engineering analysis. For estimation of the boundary layer thickness on the wedge models, if the total enthalpy profile is uniform in the freestream, then the $h_{oe} = 0.995\, h_o$ location away from the wall is determined as the boundary layer edge. On the other hand, if there is a nonuniform total enthalpy profile in the freestream, then freestream total enthalpy at the leading edge location of the model is used as the reference enthalpy. In other words, $h_{oe} = 0.995\, h_{ocl}$ when the model leading edge is at the nozzle centerline, and $h_{oe} = 0.995\, h_{ole}$ when the wedge is at an off-centerline location.

Figure 13 shows computed boundary layer profiles at the wedge plate leading edge and the sensitivity of the estimated boundary layer thickness to the reference enthalpy. As seen in Fig. 13a, there are gradients in all flow properties, the species mass fractions, magnitude of velocity, Mach number, and temperature field within and outside the boundary layer. Note that these gradients normal to the wall are due to a combination of viscous effects and the total enthalpy profile prescribed at the nozzle inlet, and also to the curved shock wave in front of the wedge model. However, it is important to note that the gradients in the flow properties near the wall are much larger than

the gradients caused by a nonuniform enthalpy profile and a curved shock wave. Figure 13b shows the sensitivity of the estimated boundary layer thickness to the reference enthalpy.

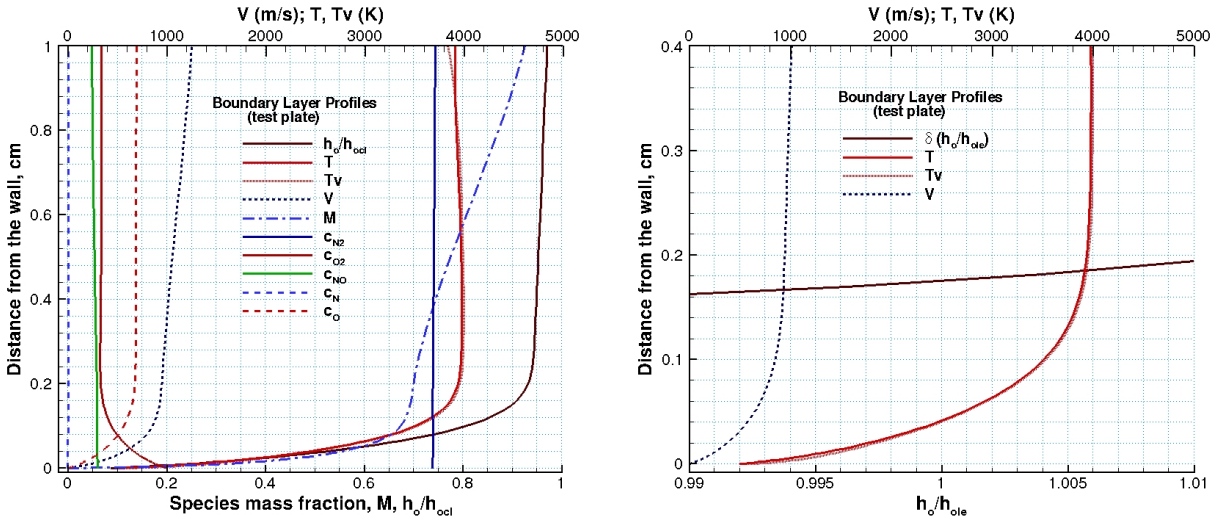

(a) at the plate leading edge **(b) sensitivity to the reference enthalpy**

Figure 13. Computed boundary layer profiles and boundary layer thickness determination on the 45° wedge test plate. TP3 7.5-inch nozzle flow: $\dot{m}$ = 296 g/s, h_{ob} = 6.0 MJ/kg, h_{ocl} = 8.1 MJ/kg.

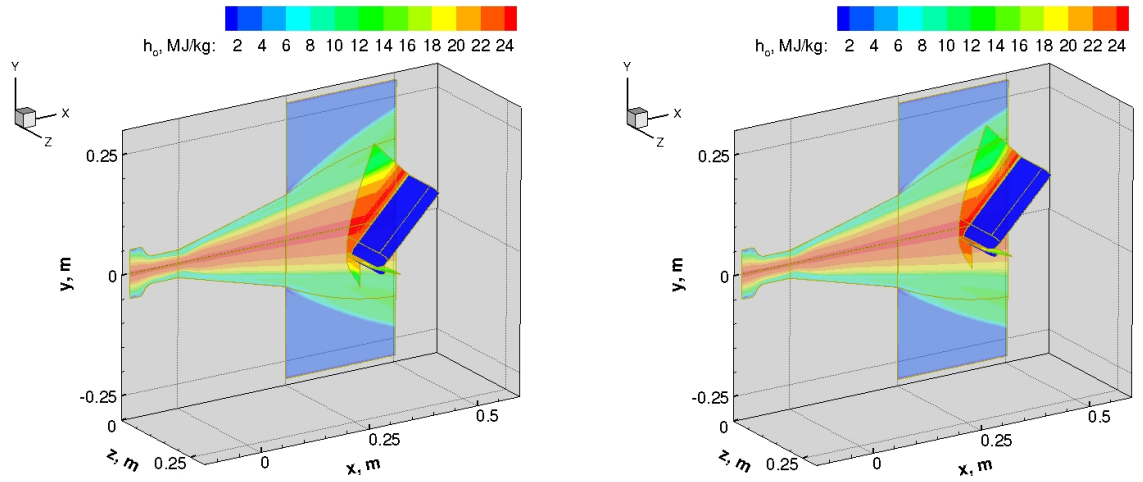

(a) 5.72 cm below the centerline **(b) 1.91 cm below the centerline**

Figure 14. Computed total enthalpy flowfield contours of the TP3 7.5-inch nozzle flow with the 45° wedge model: $\dot{m}$ = 440 g/s, h_{ob} = 13.7 MJ/kg, h_{ocl} = 24.3 MJ/kg, p_{box} = 2 torr.

The second wedge example is also from the 7.5-inch nozzle flow, and for this case, the wedge model was tested at a different off-centerline location from the first wedge case (15.24 cm downstream of the nozzle exit and 1.91 cm below centerline) but at a much higher enthalpy than the first case. As mentioned earlier, testing wedge articles at the nozzle centerline or at some distance from the nozzle centerline is a trade-off between various competing factors. Testing the models at the nozzle centerline is usually employed because of flow symmetry, and characterization of the test flow is often accomplished through stagnation calorimeters at the nozzle centerline. Also, when the total enthalpy profile is highly peaked at the centerline, the model leading edge experiences much higher enthalpy when it

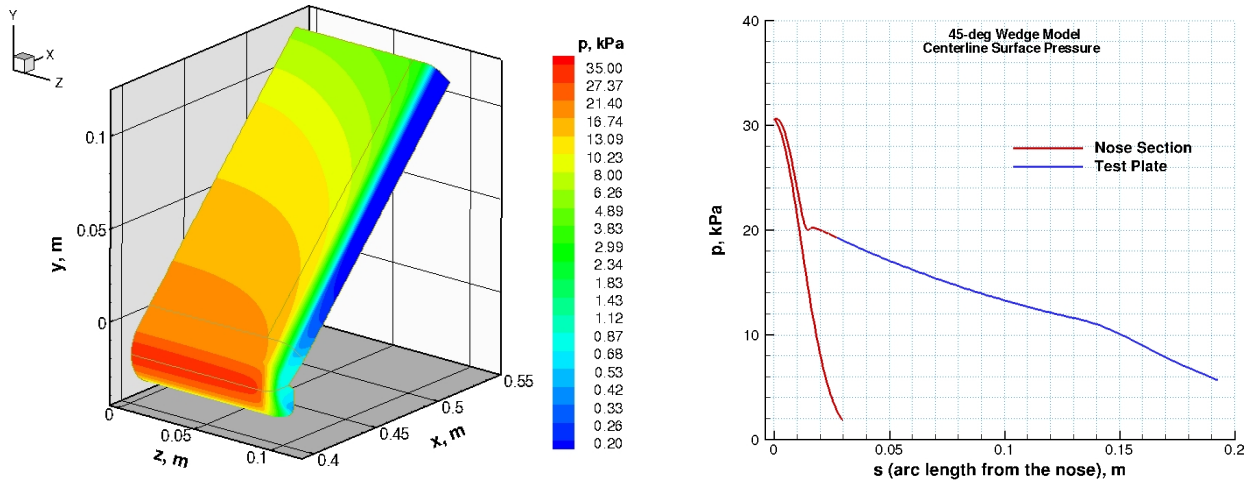

(a) pressure

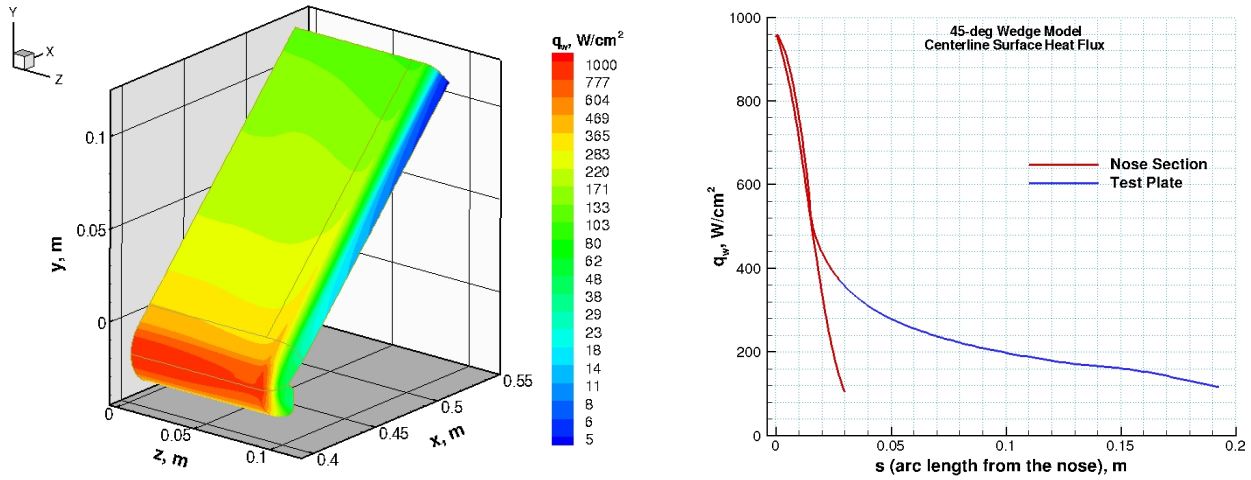

(b) heat flux

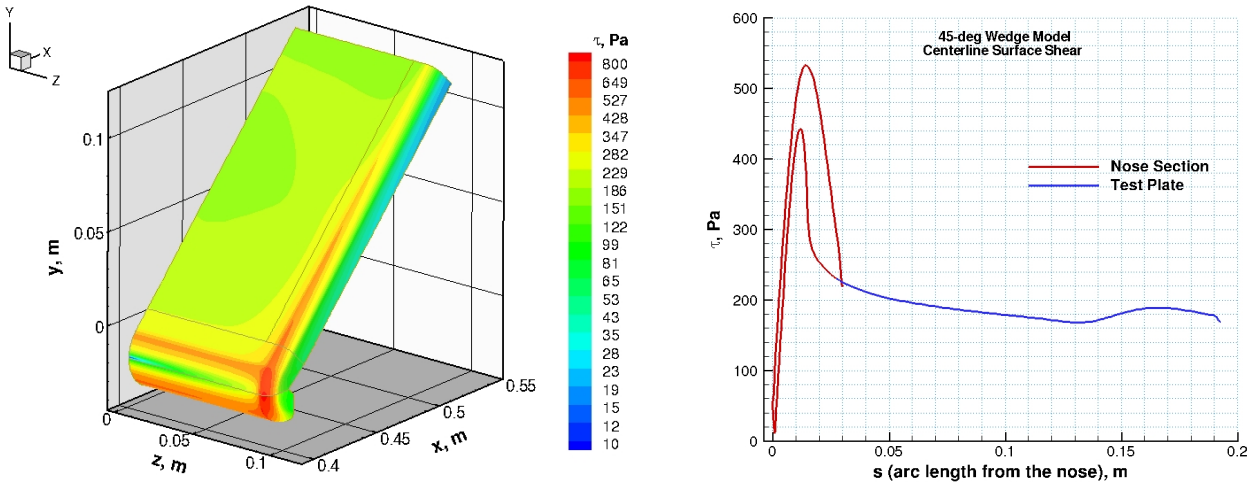

(c) shear

Figure 15. Computed surface quantities of the 45° wedge model. TP3 7.5-inch nozzle flow: $\dot{m}$ = 440 g/s, h_{ob} = 13.7 MJ/kg, h_{ocl} = 24.3 MJ/kg.

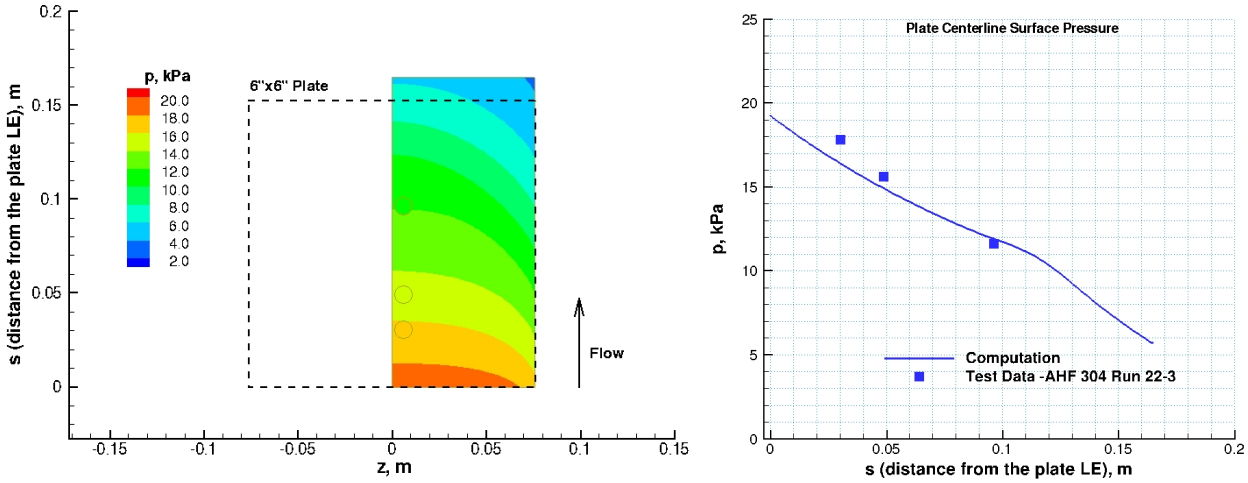

(a) pressure

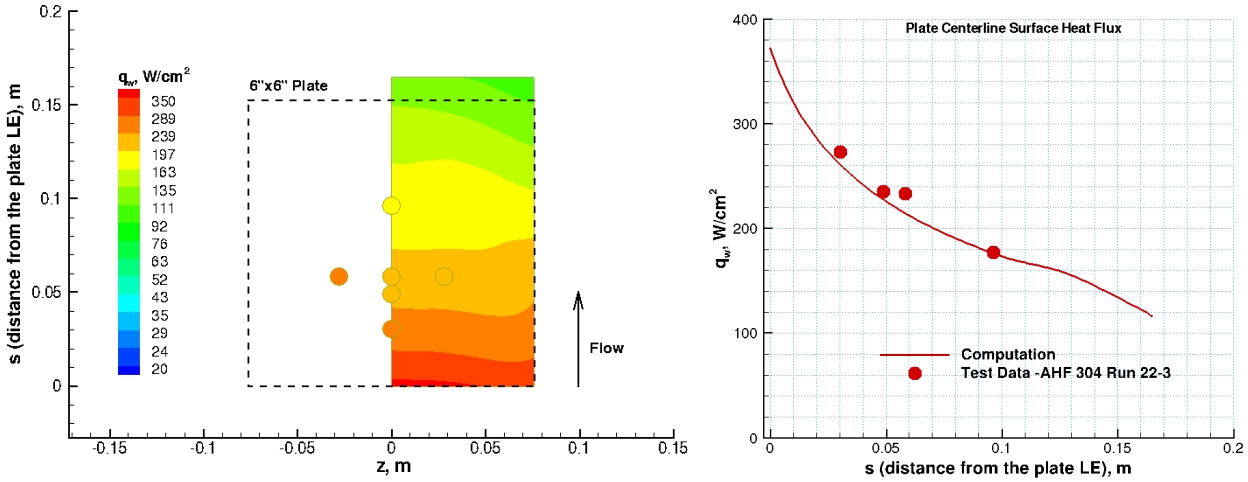

(b) heat flux

Figure 16. Comparisons of computed surface pressure and heat flux of the calibration plate with the test data for the 45° wedge model. TP3 7.5-inch nozzle flow: $\dot{m}$ = 440 g/s, h_{ob} = 13.7 MJ/kg, h_{ocl} = 24.3 MJ/kg.

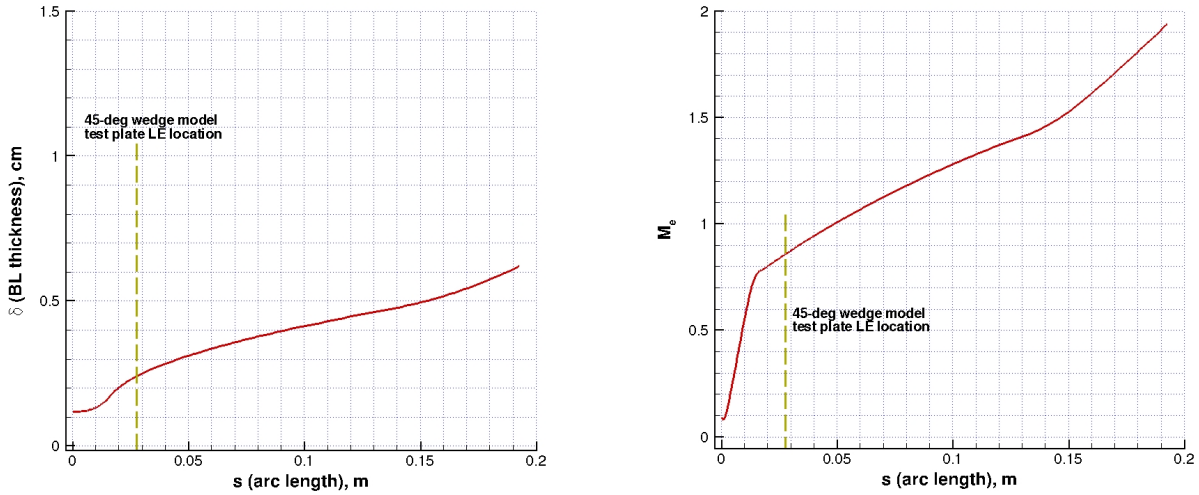

Figure 17. Computed boundary layer thickness and edge Mach number along the 45° wedge model centerline. TP3 7.5-inch nozzle flow: $\dot{m}$ = 440 g/s, h_{ob} = 13.7 MJ/kg, h_{ocl} = 24.3 MJ/kg.

is placed near the nozzle centerline. Figure 14 shows computed contours of total enthalpy for the 7.5-inch nozzle and the wedge model at two different vertical testing locations. As clearly shown in Fig. 14, the wedge model leading edge encounters a higher enthalpy when tested closer to the nozzle centerline but also a larger section of the test plate is then affected by the nozzle exit expansion waves. Only the case of 1.91 cm off centerline will be discussed further as follows.

Figures 15 and 16 show contours of the computed surface quantities of the wedge model, calibration plate and their centerline profiles, with the model leading edge 1.91 cm below the centerline. These plots are similar to those in Figs. 10-11 where the leading edge was 5.72 cm below centerline. However, as the surface contours show, the extent of asymmetry in the wedge surface quantities near the nose section is smaller than that of the first wedge case since the wedge leading edge is closer to the nozzle centerline. Consequently, interaction of the expansion waves from the nozzle exit with the shock wave is also much more pronounced, thus disturbing the shock shape and perturbing the uniformity at the wedge surface. Significant gradients observed in the surface quantities of the wedge model, from the contour plots and slope changes in the centerline line plots at about 10 cm from the plate leading edge, are manifestations of the nozzle-lip expansion and wedge shock wave interactions. Again, the agreement in the computed and measured pressure and heat flux distributions along the plate centerline, as shown in Fig 16, indicates that expansion wave interaction and other three dimensional effects are adequately captured by the computations.

Figure 17 shows the corresponding distributions of the predicted boundary layer thickness and edge Mach number along the model centerline. For this case, a subsonic boundary layer edge Mach number at the plate leading edge was one of the test requirements, and it is verified through these CFD simulations.

ii. TP3 20-inch nozzle flow/wedge model simulations

A limited number of large wedge (36.83 cm width) tests were run in the 20-inch nozzle. One case from the large wedge simulations is presented. For this case, the leading edge of the wedge model was on centerline and at 15.24 cm downstream of the nozzle exit plane. Nominal surface heat flux and pressure ranges required for the test plate were 2.5-7 W/cm^2 and 0.07-0.5 kPa. These relatively low heat and pressure ranges are typically suited for the Panel Test Facility (PTF) supersonic semi-elliptical nozzle flow.[3] However, achieving a subsonic boundary layer edge Mach number at the test plate leading edge was one of the test requirements, which cannot be simulated in the PTF. In fact, the wedge half-angle for this case was raised to 50 degrees to achieve a subsonic boundary layer edge. Note that the 45° wedge angle that was used in the 7.5-inch nozzle tests was not sufficient in the 20-inch nozzle because of the higher freestream Mach number and differences in test plate locations of the two wedge models.

Figure 18 shows contours of the computed surface quantities (pressure, heat flux, and shear) of the large wedge model and their centerline profiles. Although these are similar to the surface contours of the small wedge model shown in Figs. 10 and 15, there are some qualitative differences. The nose radius of the large wedge model is one half of the nose radius of the small wedge model, and the test plate location for the large wedge model was much further from the nose section than that of the small wedge model. Also, the freestream Mach numbers for the 7.5-inch and 20-inch nozzles are about 4.4 and 6.7, respectively. Because of the smaller nose radius, and the greater test plate distance away from the nose section, the gradients in the test plate surface quantities for the large wedge model are much lower at the test plate leading edge than the small wedge test plate. However, at the location where the nozzle lip expansion wave interaction with the wedge shock wave starts, gradients in the surface quantities increase significantly, e.g., as seen in the surface pressure at about 0.19 m from the leading edge in Fig. 18c.

Figure 19 shows comparisons of computed calibration-plate surface quantities with the test data. Unfortunately, there were some issues in both heat flux and pressure measurements on the calibration plate, attributed to difficulty in measuring relatively low surface heat flux and pressure levels. Also, the calibration plate covered only a smaller section of the nominal test plate area, so it is not possible to establish trends in the measured data. However, the available data and computations indicate that the test requirements can be met within the given ranges. It is worth mentioning that computational results show that there are strong expansion wave/shock wave interactions present for this case, as evidenced by the nonuniform surface contours and line plots in Figs. 19a and 19b.

Finally, Fig. 20 shows the corresponding distributions of the predicted boundary layer thickness and edge Mach number along the large wedge model centerline. For this case, CFD simulations confirm that a subsonic boundary layer edge Mach number at the plate leading edge was achieved with the 50° wedge angle.

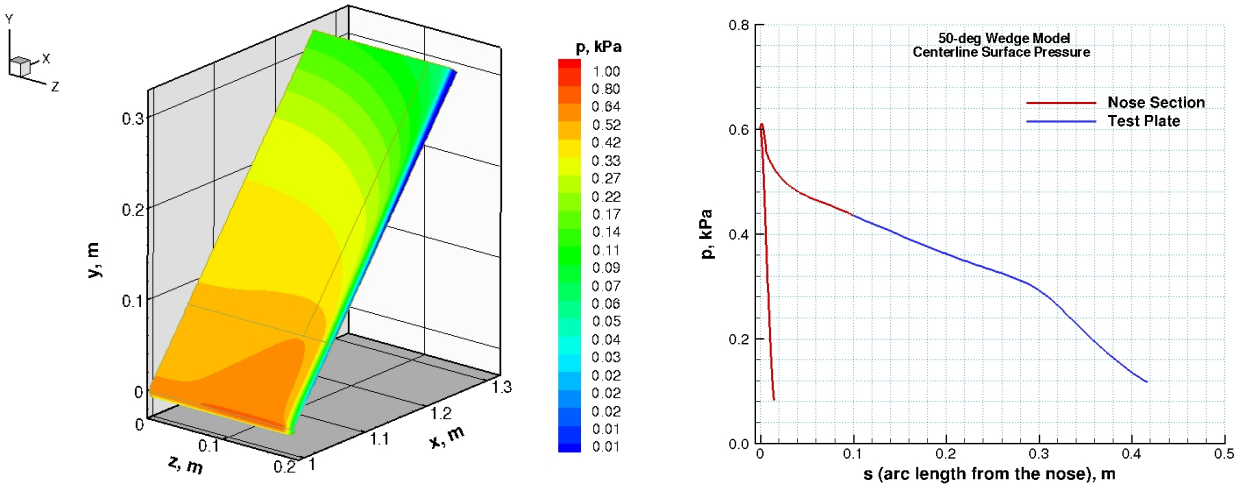

(a) pressure

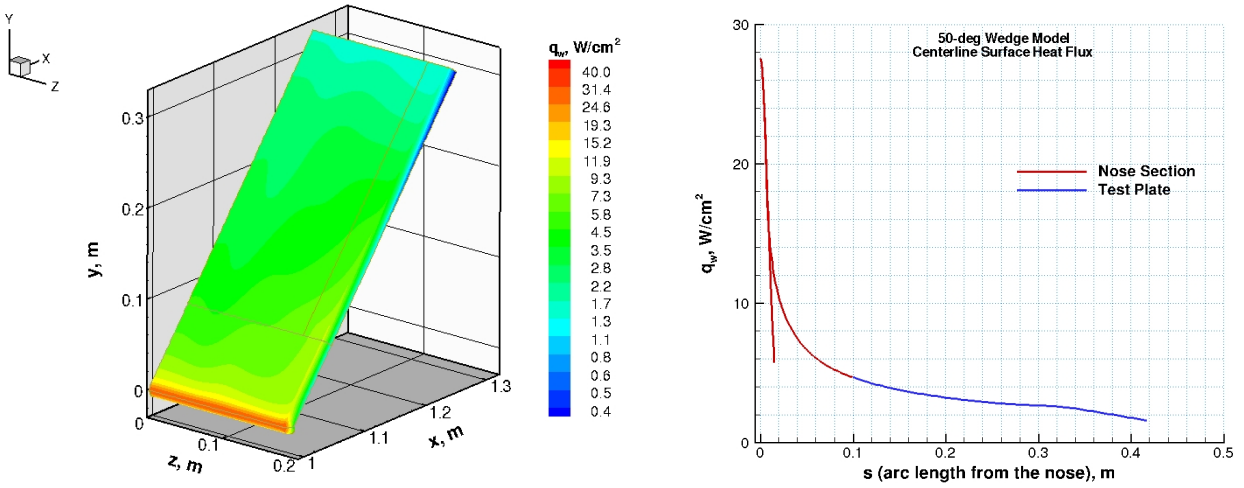

(b) heat flux

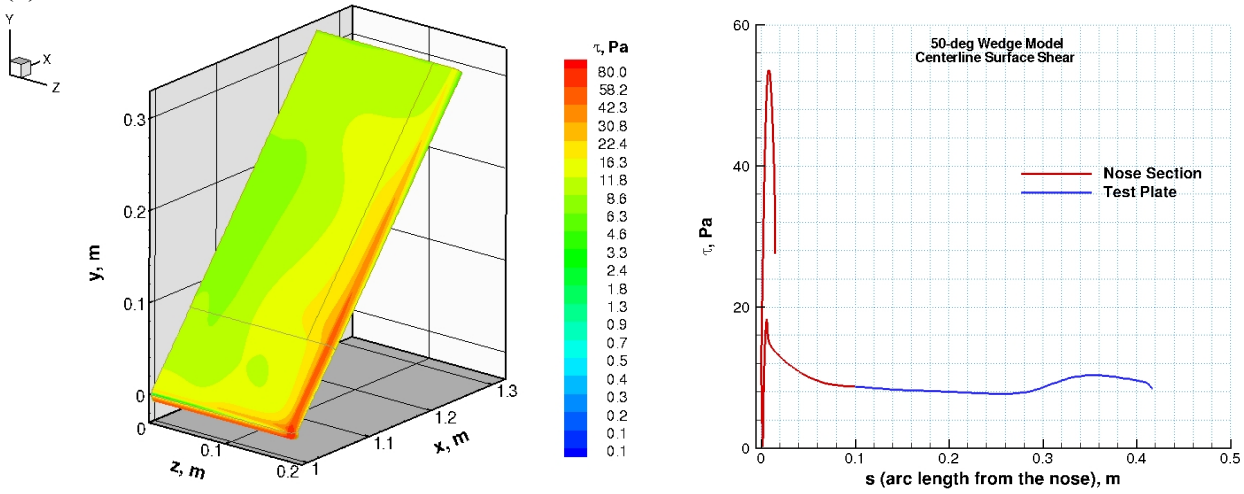

(c) shear

Figure 18. Computed surface quantities of the 50° wedge model. TP3 20-inch nozzle flow: $\dot{m}$ = 74 g/s, h_{ob} = 4.5 MJ/kg, h_{ocl} = 5.4 MJ/kg.

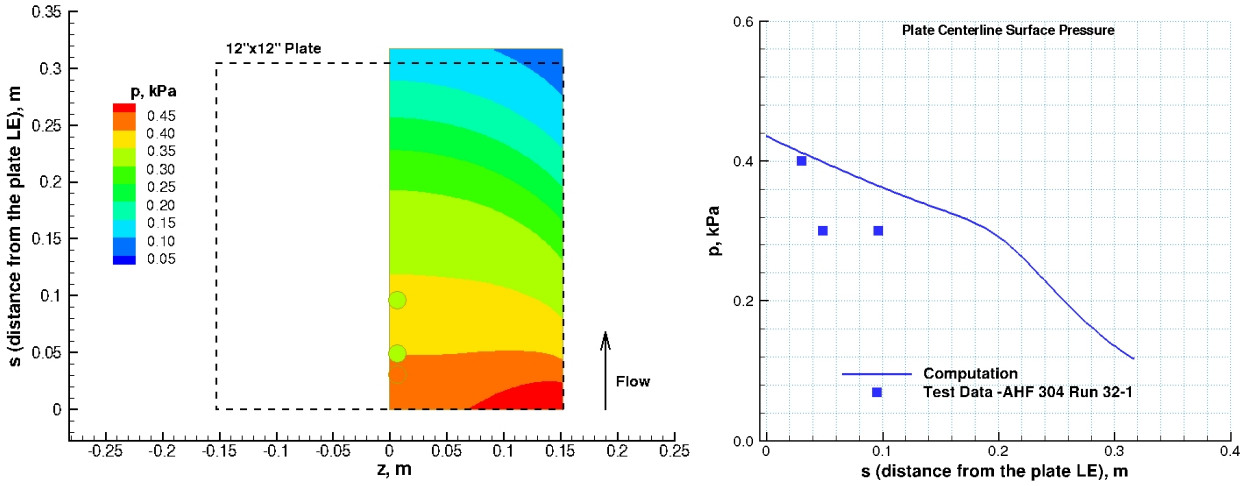

(a) pressure

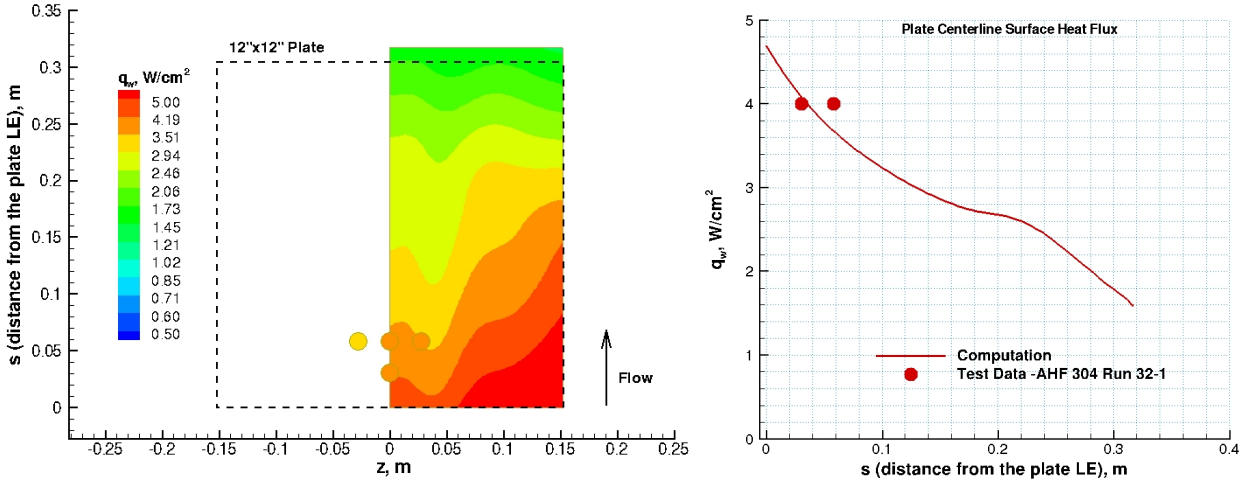

(b) heat flux

Figure 19. Comparisons of computed surface pressure and heat flux of the calibration plate with the test data for the 50° wedge model. TP3 20-inch nozzle flow: $\dot{m}$ = 74 g/s, h_{ob} = 4.5 MJ/kg, h_{ocl} = 5.4 MJ/kg.

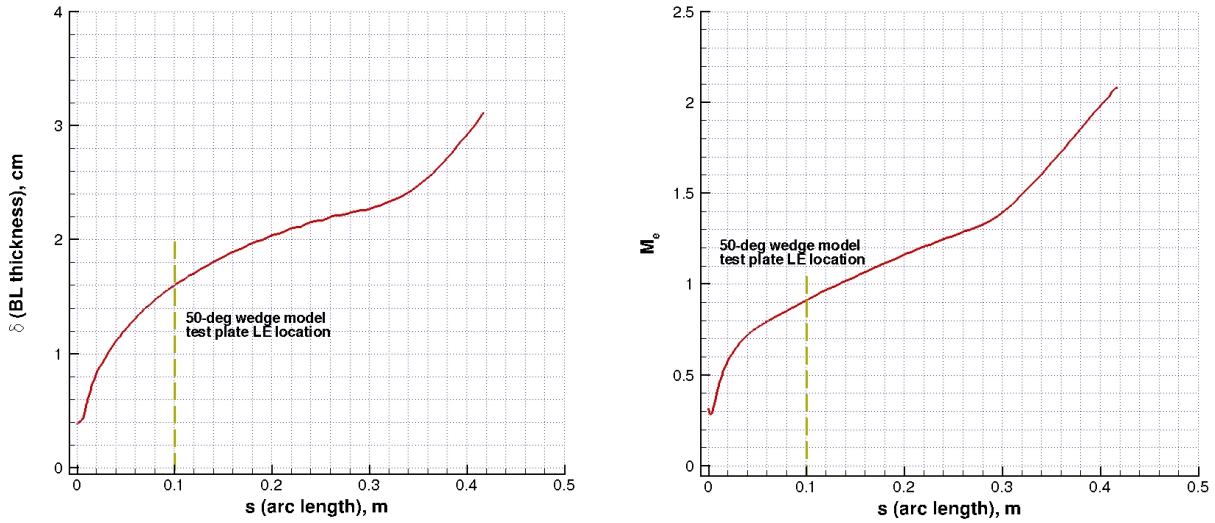

Figure 20. Computed boundary layer thickness and edge Mach number along the 50° wedge model centerline. TP3 20-inch nozzle flow: $\dot{m}$ = 74 g/s, h_{ob} = 4.5 MJ/kg, h_{ocl} = 5.4 MJ/kg.

V. Concluding Remarks

Computational simulations in support of arc-jet tests in the NASA Ames 10-MW TP3 arc-jet facility flow are presented. The test data included heat flux and pressure measurements with stagnation calorimeters, measurements of surface pressure and heat flux on calibration plates integrated with two wedge models, and surveys of arc-jet test flow with pitot and null-point heat flux probes. The probe survey data obtained at several arc-heater conditions provide assessment of the flow uniformity and valuable data for the flow characterization. Computations of the nonequilibrium flowfield in the nozzle, test box, and over the test articles, are performed. These simulations take into account nonuniformities in the total enthalpy and mass flux profiles at the nozzle inlet as well as the expansion waves emanating from the nozzle exit and its effects on the model flowfields, and they predict model surface pressure and heat flux measurements consistent with the set of arc-jet facility data.

Computational simulations, through comparisons with the test data, provide estimates of arc-jet test environment parameters, the centerline total enthalpy being the most important test parameter. CFD results also provide the only means to estimate certain test environment parameters such as boundary layer thickness, edge Mach number, and surface shear, which are often critical parameters to assess TPS behavior. As part of the specified Orion CAT requirements, these environment parameters are verified through CFD simulations since they cannot be measured. During the CAT program, a comprehensive set of arc-jet test data with supporting CFD simulations were obtained. Following successful completion of the CAT program, the 10-MW TP3 arc-jet is now operational and will continue to support future Orion TPS testing.

As demonstrated in earlier work for other Ames arc-jet facilities, these computational simulations for TP3 can assist test planning, define arc-jet test environments for surface properties of TPS, reduce exploratory testing, and provide a framework for tracing the TPS performance from this ground test facility to flight.

Acknowledgments

This work was funded by the NASA Arc Jet Consolidation and Orion TPS Insight/Oversight projects. The arc-jet operational capability at NASA ARC is also supported by NASA-SCAP. The authors would like to thank all of the facilities staff involved in the TP3 tests, in particular, test engineers Frank C. L. Hui and Imelda Terrazas-Salinas. The support from the NASA Ames Entry Systems and Technology Division, through contract NNA10DE12C to ERC, Inc., is gratefully acknowledged.

References

[1]Rochelle, W. C., Battley, H. H., Grimaud, J. E., Tillian, D. J., Murray, L. P., Lueke, W. J., and Heaton, T. M., "Orbiter TPS Development and Certification Testing at the NASA/JSC 10 MW Atmospheric Reentry Materials and Structures Evaluation Facility," AIAA-83-0147, Jan. 1983.

[2]Balboni, J. A., Gökçen, T., Hui, F. C. L., Graube, P., Morrissey, P., Lewis, R. "Consolidating NASA's Arc-Jets," AIAA Paper 2015-2667, AIAA Aviation 2015 Conferences, Dallas, Texas, June 22-26, 2015.

[3]Terrazas-Salinas, I., and Cornelison, C., "Test Planning Guide for TSF Facilities," Thermophysics Facilities Branch, Entry Systems and Technology Division, NASA Ames Research Center, Rev. C, April 2009.

[4]Wright, M. J., Candler, G. V., and Bose, D., "Data-Parallel Line Relaxation Method for the Navier-Stokes Equations," *AIAA Journal*, Vol. 36, No. 9, 1998, pp. 1603-1609.

[5]Wright, M. J., "Data-Parallel Line Relaxation Code, DPLR Version 4.02," Private Communication, June 2010.

[6]Park, C., *Nonequilibrium Hypersonic Aerothermodynamics*, John Wiley & Sons, Inc., New York, 1990, Chap. 4.

[7]Gökçen, T., Skokova, K., Balboni, J. A., Terrazas-Salinas, I., and Bose, D., "Computational Analysis of Arc-Jet Wedge Calibration Tests in IHF 6-Inch Conical Nozzle," AIAA Paper 2009-1348, Jan. 2009.

[8]Saunders, D. A., and Gökçen, T., "Nozzle Throat Conditions for Arc-Jet Computations: (1) Axisymmetric," ELORET Report TSA-01-DB2-1-2008, Oct. 2008.

[9]Gökçen, T., Chen, Y. K., Skokova, K. A., and Milos, F. S., "Computational Analysis of Arc-Jet Stagnation Tests Including Ablation and Shape Change," *Journal of Thermophysics and Heat Transfer*, Vol. 24, No. 4, 2010, pp. 694-707; also AIAA Paper 2009-3596, June 2009.

[10]Gökçen, T., and Alunni, A. I., "On Laminar to Turbulent Transition of Arc-Jet Flow in the NASA Ames Panel Test Facility," *Journal of Thermophysics and Heat Transfer*, Vol. 27, No. 3, July-September 2013, pp. 549-562; also AIAA Paper 2012-3304, June 2012.

[11]Terrazas-Salinas, Carballo, J. E., I., Driver, D. M., and Balboni, J. A., "Comparison of Heat Transfer Measurement Devices in Arc Jet Flows with Shear," AIAA Paper 2010-5053, June 2010.

[12]Pope, R., B., "Measurements of Enthalpy in Low-Density Arc-Heated Flows," *AIAA Journal*, Vol. 6, No. 1, 1968, pp. 103-110.

[13]Saunders, D. A., "CFD Utilities: BLAYER program," sourceforge.net/projects/cfdutilities/BLAYER, March 2015.